Thesis for the Degree of Licentiate of Engineering

Nonlinearity mitigation in phase-sensitively amplified optical transmission links

Kovendhan Vijayan

CHALMERS

Photonics Laboratory
Department of Microtechnology and Nanoscience
Chalmers University of Technology
Göteborg, Sweden, 2019

Nonlinearity mitigation in phase-sensitively amplified optical transmission links
Kovendhan Vijayan

ISSN 1652-0769
Technical Report MC2-424

Chalmers University of Technology
Department of Microtechnology and Nanoscience - MC2
Photonics Laboratory
SE–412 96 Göteborg
Sweden
Phone: +46–(0)31–772 10 00

Front cover illustration: Measured constellation diagrams showing XPM and SPM mitigation using PSAs.

Printed in Sweden by
Reproservice
Chalmers Tekniska Högskola
Göteborg, Sweden, 2019

Nonlinearity mitigation in phase-sensitively amplified optical transmission links

Kovendhan Vijayan
Photonics Laboratory
Department of Microtechnology and Nanoscience
Chalmers University of Technology

Abstract

The fundamental limitations in fiber-optic communication are caused by optical amplifier noise and the nonlinear response of the optical fibers. The quantum-limited noise figure of erbium-doped fiber amplifier (EDFA) or any phase-insensitive amplifier is 3 dB. However, the noise added by the amplification can be reduced using phase-sensitive amplifier (PSA) whose quantum-limited noise figure is 0 dB. PSAs can also compensate for the nonlinear distortions from the optical fiber with copier-PSA implementation. At the transmitter, a copier which is nothing but a phase-insensitive amplifier is used to create a conjugated copy of the signal. The signal and idler are co-propagated in the span, experiencing correlated nonlinear distortions. The nonlinear distortions are reduced by the all-optical coherent superposition of the signal and idler in the PSA.

In this work, an analytical investigation is performed for the nonlinearity mitigation using the PSAs, by calculating the residual nonlinear distortion after the coherent superposition in PSAs. The optical bandwidth and the dispersion map dependence on the nonlinearity mitigation in the PSAs are analytically and experimentally studied. A modified Volterra nonlinear equalizer (VNLE) is used to reduce the residual nonlinear distortions after PSAs. Experiments were performed to show that PSAs can mitigate cross-phase modulation (XPM), which was evident by observing the constellation diagrams. The maximum allowed launch power increase was also measured to quantify the XPM mitigation. To the best of our knowledge, this is the first experiment that showed the mitigation of XPM in a phase-sensitively amplified transmission link. Also, the effectiveness in mitigating self-phase modulation (SPM) and XPM using a PSA is studied.

Keywords: optical transmission, nonlinearity mitigation, phase-sensitive amplifier, low-noise amplification, self-phase modulation mitigation, cross-phase modulation mitigation, copier-PSA

Publications

This thesis is based on the work contained in the following papers:

[A] B. Foo, M. Karlsson, **K. Vijayan**, M. Mazur, and P. A. Andrekson, "An Analysis of Nonlinearity Mitigation Using Phase-Sensitive Optical Parametric Amplifiers", *Optics Express*, vol. 27, no. 22, pp. 31926-31941, October 2019.

[B] **K. Vijayan**, H. Eliasson, B. Foo, S. L. I. Olsson, M. Karlsson, and P. A. Andrekson, "Optical Bandwidth Dependency of Nonlinearity Mitigation in Phase-Sensitive Amplifier Links", in *European Conference on Optical Communication (ECOC)*, Sept 2018.

[C] **K. Vijayan**, B. Foo, M. Karlsson, and P. A. Andrekson, "Long-haul Transmission of WDM Signals With In-Line Phase-Sensitive Amplifiers", in *European Conference on Optical Communication (ECOC)*, Sept 2019.

[D] **K. Vijayan**, B. Foo, M. Karlsson, and P. A. Andrekson, "Cross-Phase Modulation Mitigation in Phase-sensitive Amplifier Links", *IEEE Photonics Technology Letters*, **Accepted - Early Access**, Sept 2019 **(DOI: 10.1109/LPT.2019.2944100)**.

Related work by the author (not included in this thesis):

[E] R. Kakarla, **K. Vijayan**, A. Lorences-Riesgo, and P. A. Andrekson "High Sensitivity Receiver Demonstration Using Phase Sensitive Amplifier for Free-Space Optical Communication", in *European Conference on Optical Communication (ECOC)*, Sept 2017.

[F] R. Kakarla, **K. Vijayan**, J. Schröder, and P. A. Andrekson "Phase Noise Characteristics of Injection-Locked Lasers operated at Low Injection Powers", in *Optical Fiber Communication Conference (OFC)*, March 2018.

[G] H. Eliasson, **K. Vijayan**, B. Foo, S. L. I. Olsson, E. Astra, M. Karlsson, and P. A. Andrekson, "Phase-Sensitive Amplifier Link With Distributed Raman Amplification", *Optics Express*, vol. 26, no. 16, pp. 19854-19863, August 2018.

[H] **K. Vijayan**, B. Foo, H. Eliasson, and P. A. Andrekson "Cross-Phase Modulation Mitigation in WDM Transmission Systems Using Phase-Sensitive Amplifiers", in *European Conference on Optical Communication (ECOC)*, Sept 2018.

Contents

Acknowledgement

First and foremost, I like to thank my supervisors Prof. Peter Andrekson and Prof. Magnus Karlsson for accepting me as a PhD student in the PSA group. Their guidance and support have been the backbone of this work. Dr Jochen Schröder deserves a special thanks for always being there to help me with my presentations and reports. I like to thank Ravikiran Kakarla and Dr Samuel Olsson for helping me understand the basics of PSAs. Dr Abel Lorences-Riesgo deserves a special thanks for teaching me how to implement the PSAs experimentally for the first time. I like to thank Dr Henrik Eliasson for introducing me to the PSA-loop experiments, teaching me about Raman amplification and introducing me to the cluster simulations. Dr Ben Foo with whom I had the privilege to work in the lab deserves a special thanks for all the help, fruitful discussions and his contribution to this work. In the last two years, he has been the to-go person for any kind of help in the simulations and DSP for me. Ali Mirani deserves a special thanks for the exciting discussions on communication theory. Jeanette Träff deserves a special thanks for helping with all the administrative stuff. I also like to thank all the other photonics laboratory members for the nice discussions and work environment.

I like to thank all my friends and family members who had made my life outside research. I also like to thank the photonics lab members for all the ping-pong games. Last but not least, I would like to express my deepest gratitude to my wife Nisha, whose support has been vital. I also like to thank my parents and sister for all their support and care.

I also like to thank the Swedish Research Council for the financial support.

Kovendhan Vijayan

Göteborg
October 2019

Acronyms

EDFA	erbium-doped fiber amplifier
PSA	phase-sensitive amplifier
VNLE	Volterra nonlinear equalizer
XPM	cross-phase modulation
SPM	self-phase modulation
WDM	wavelength-division multiplexing
DCF	dispersion compensating fiber
FBG	fiber Bragg grating
DCM	dispersion compensation module
HNLF	highly nonlinear fiber
OPC	optical phase conjugation
PCTW	phase-conjugated twin wave
DBP	digital back-propagation
SSMF	standard single-mode fiber
PMD	polarization-mode dispersion
GVD	group-velocity dispersion
PMF	polarization-maintaining fiber
SOP	principal states of polarization
CW	continuous wave
ZDW	zero-dispersion wavelength
XpolM	cross-polarization modulation
FWM	four-wave mixing
SBS	stimulated Brillouin scattering
FOPA	fiber-optic parametric amplifier
BPSK	binary phase-shift keying
QPSK	quadrature phase-shift keying
PLL	phase-locked loop
SRS	stimulated Raman scattering
NLSE	nonlinear Schrödinger equation

SSFM	split-step Fourier method
SOA	semiconductor optical amplifier
ASE	amplified spontaneous emission
NF	noise figure
SNR	signal-to-noise ratio
AQN	amplified quantum noise
PS	phase-sensitive
PI	phase-insensitive
FOM	figure of merit
EDC	electronic dispersion compensation
DAC	digital-to-analog converter
PIA	phase-insensitive amplifier
PTN	pump-transferred noise
PAM	pulse-amplitude modulation
OIL	optical-injection locking
NLPN	nonlinear phase noise

Chapter 1

Introduction

Almost everything in this world is connected to the internet. The internet users, the internet-based applications and the number of devices using the internet are increasing every day. According to Cisco, the monthly global IP traffic in 2017 was 122 Exabytes and is predicted to reach 396 Exabytes by 2022 [1], as shown in figure 1.1. Moreover, the global internet users will make up to 60% of world's population and the number of connected devices will reach 28.5 billion by 2022. Fiber-optic communication acts as the backbone to these networks. The various inventions in the field of optical communications have paved way to meet these data traffic demands.

The first historic event in the field of optical communication is the transmission of the sound signals over a distance of 200 m with sunlight as the optical carrier by Alexander Graham Bell known as the 'photophone' [2]. However, this did not create a significant impact in the field of communication at that time due to the lack of a reliable intense light source. The realization of the first laser in 1960 [3], lead to an increase in research on topics of optical devices, components, and signal-processing techniques. On a large scale, even initiated research on the subsystems including the transmission media, which consisted of periodic focusing elements [4] as the available glass fibers were found to have losses of 1000 dB/km. This marked the beginning of the current optical communications research. The first proposal to use clad glass fiber for transmitting information in telecommunication industry came in 1966 [5] with the announcement of doped silica fiber having a loss of 20 dB/km [6] in 1970. The losses in the silica fiber were reduced to 0.2 dB/km in 1979 at 1.55 μm [7] making it the best medium for long-distance communication.

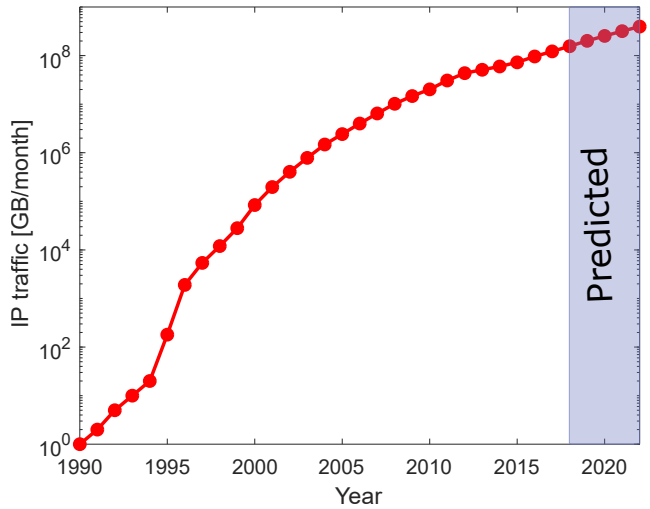

Figure 1.1: Evolution of the IP data traffic over the years (adopted from [1]).

The next major break-through in optical communication is the invention of erbium-doped fiber amplifier (EDFA) in 1986 [8]. The introduction of EDFAs not only removed the need for repeaters in the fiber-optic communication links but also provided the ability to use wavelength-division multiplexed (WDM) signals. However, then the bottleneck was the dispersion, which was overcome with the help of dispersion compensating fibers (DCFs) [9] or fiber Bragg grating (FBG)-based dispersion compensation modules (DCMs) [10]. The amount of transmitted information can be increased further by encoding the information not only in amplitude of the optical wave but also in phase using coherent communication systems. However, this needs the detection of both amplitude and phase of the received signal. Coherent communication enabled the usage of higher-order modulation format increasing the amount of transmitted information. Also, the impairments in the transmission system can be compensated in the digital domain by signal processing after detection in the coherent systems. These inventions made it possible to meet the ever-increasing demands in data transmission.

Moving on to a more fundamental level of the fiber-optic communication systems, one of the main limitations is the noise from the optical amplifier. As the optical wave travels inside the optical fiber, the small loss of 0.2 dB/km attenuates the signal. These losses have to be overcome through the process of optical amplification with the optical

amplifiers, which also adds some noise to the signal. The most common amplifier used in optical communications is the EDFA which is a phase-insensitive amplifier (PIA). The gain in the PIAs is independent of the signal phase. There is a special kind of amplifier known as the phase-sensitive amplifiers (PSAs) adding 3 dB less noise theoretically compared to the PIAs [11]. In this thesis, the PSAs based on highly nonlinear fibers (HNLFs) are used as the optical amplifiers to add less noise to the signal compared to the EDFAs.

The other major limitation is the Kerr effect in the optical fiber. The nonlinear distortions due to the fiber nonlinearities can be compensated in the optical domain by using optical phase conjugation (OPC) [12]. The signal is phase-conjugated in the mid of the transmission span, to compensate for the dispersion and nonlinearities from the first part of the span. The other technique to compensate the nonlinearities is by performing coherent superposition of the signal and the phase-conjugate copy of the signal in the digital domain after detection known as the phase-conjugated twin waves (PCTW) [13]. However, the copier-PSA is capable of doing the same in the optical domain and at the same time adding less noise to the signal. In this thesis, an analytical model has been obtained that describes the nonlinearity compensation in the copier-PSA. Also, several experiments have been performed to study the effectiveness of nonlinearity mitigation in PSAs. In the digital domain after detection, digital back-propagation (DBP) [14] and Volterra nonlinear equalizers (VNLE) [15] are mostly used to compensate for nonlinear distortions. The digital and optical domain techniques can also be used together. It is also been shown in this thesis that the residual nonlinear distortions after the coherent superposition in the PSAs can be further reduced by using a modified Volterra nonlinear equalizer.

Further in this thesis, the various impairments when the optical wave travels in the optical fibers are explained in chapter 2. The optical amplification and dispersion compensation used to overcome the linear impairments are discussed in chapter 3. A detailed study on parametric amplifiers based on optical fibers is performed in chapter 4. The phase-sensitive amplifiers in different configurations are studied in chapter 5. In chapter 6, the various optical and digital methods to compensate nonlinear impairments are listed. In particular, a detailed analysis is performed for nonlinearity mitigation using PSAs. The papers are summarized in chapter 7.

Chapter 2

Wave Propagation in Optical fibers

The main physical effects in an optical fiber that affect the optical field during propagation can be categorized into the linear effects and nonlinear effects. At low optical powers, the nonlinear effects can be neglected. The linear effects occur independently for each frequency component in the fiber and are not affected by the presence of optical waves at other frequencies. As the optical power is increased, the nonlinear effects become important. The nonlinear effects are capable of changing the properties of the optical waves at other frequencies or can even create a new frequency wave. In this chapter, these effects are explained with respect to the standard single-mode fiber (SSMF) used for data transmission and the HNLF that is used as parametric amplifiers in this work.

2.1 Linear effects

The linear effects affecting the wave propagation in the optical fibers are attenuation, dispersion and polarization-mode dispersion (PMD).

2.1.1 Fiber attenuation

Optical fibers made from silica are extremely transparent and therefore is used as a medium for long-distance communication with light. For long-haul communication, the C-band spanning from 1530-1570 nm is used in the optical fiber where the attenuation is mainly caused by Rayleigh scattering and material absorption. As the optical wave propagates in

the fiber, the evolution of the optical power can be modelled with Beer's law as

$$P(z) = P(0)\exp(-\alpha z), \tag{2.1}$$

where α is the attenuation coefficient in linear units. It is common to represent α in units of dB/km known as the fiber-loss parameter (α [dB/km]). For a SSMF and a HNLF, the fiber-loss parameters are 0.2 dB/km and 0.6 - 1.2 dB/km, respectively. The fiber-loss parameter can be assumed constant over the communication window as their variation is minimal. An ultra-low loss optical fiber with α of 0.14 dB/km has been reported in [16].

2.1.2 Dispersion

The wavelength-dependent refractive index of the optical fiber due to material properties and waveguide design causes different frequencies of the optical wave to travel with different velocities leading to group-velocity dispersion (GVD), also known as dispersion. Dispersion changes the temporal shape of the pulse during propagation in the optical fiber. In the frequency domain, the linear propagation of an optical field can be modelled as

$$\tilde{E}(z,\omega) = \tilde{E}(0,\omega)\exp i\beta(\omega)z, \tag{2.2}$$

where $\beta(\omega)$ is the propagation constant:

$$\beta(\omega) = \frac{n(\omega)\omega}{c}, \tag{2.3}$$

where $n(\omega)$ is the refractive index and c is the velocity of light in vacuum. To account for the frequency dependence of the propagation constant, the propagation constant can be expanded using a Taylor series around the carrier frequency (ω_0) as

$$\beta(\omega) = \beta_0 + \beta_1(\omega-\omega_0) + \frac{\beta_2}{2}(\omega-\omega_0)^2 + \frac{\beta_3}{6}(\omega-\omega_0)^3 + \ldots, \tag{2.4}$$

where $\beta_i \equiv \left.\frac{d^i\beta}{d\omega^i}\right|_{\omega=\omega_0}$ is the Taylor expansion coefficients. β_0 corresponds to the phase velocity of the carrier wave by $v_p = \frac{\omega_0}{\beta_0}$ and the group velocity at the carrier frequency (v_g) is related to β_1 as $v_g = \frac{1}{\beta_1}$. β_2 describes the frequency dependence of group velocity and is also known as the GVD parameter given in units of [ps^2/km]. The frequency dependence of the GVD is given by the third-order dispersion parameter (β_3).

However, the more commonly used are the dispersion parameter (D) in [ps/(nm km)] and the dispersion slope (S) in [ps/(nm^2 km)], which are related to the Taylor expansion coefficients as

$$D = \frac{-2\pi c}{\lambda^2}\beta_2, \tag{2.5}$$

$$S = \left(\frac{2\pi c}{\lambda^2}\right)^2 \beta_3 + \frac{4\pi c}{\lambda^3}\beta_2, \tag{2.6}$$

where λ is the wavelength of the light. In general, the higher-order terms are often neglected but should be taken into account for wide bandwidth operation. For the SSMF, the disperion parameter, $D = 18$ ps/(nm km) at 1550 nm. The dispersion parameter for the HNLF is usually less than $|0.5|$ ps/(nm km). In such cases, the dispersion slope and even the higher-order dispersion parameters should be considered. The gain-bandwidth of the parametric amplifiers are dictated by the dispersion properties of the HNLF. The variation of the dispersion properties along the fiber also affects the gain-bandwidth [17,18] and even the noise properties [19] of the parametric amplifiers.

2.1.3 Polarization-mode dispersion

Optical waves with the same frequency when launched in different polarizations into the optical fiber, travel at different group velocities known as fiber birefringence. Fiber birefringence can be random or deterministic. Polarization-maintaining fibers (PMFs) have deterministic birefringence which are manufactured with longitudinal stress rods along the fiber to have a robust linear birefringence containing a fast and a slow axis. If an input wave is launched either of the two axes, the polarization of the input wave is preserved during propagation. In case of the fiber with randomly varying birefringence, the orientation of any locally defined fast or slow axes can be considered constant only for small distances as they change randomly along the fiber. If a polarized optical wave is launched into a fiber with varying birefringence, the polarization of the optical wave changes randomly during propagation along the fiber. The polarization rotations are also frequency-dependent. There are two polarization states in the fiber where the polarization of the output wave is independent of the optical wave frequency to first-order approximation is known as the principal states of polarization (SOPs) [20]. The PMD corresponds to the difference in group velocity of the two SOPs. For the ideal SSMF, the PMD is zero due to the rotational symmetry. However,

fiber asymmetries due to non-uniformities in manufacturing, any stress or bending, environmental fluctuations in temperature, vibrations and any stress can lead to differences in the group velocities leading to randomly varying birefringence. The PMD induced differential group delay in the SSMF can be calculated as

$$\Delta t_{gp} = D_p \sqrt{L}, \tag{2.7}$$

where D_p is the PMD parameter. The typical value of (D_p) is 0.1 ps/$\sqrt{\text{km}}$. The HNLFs can be of PMFs or fibers with random birefringence. Polarization determines the strength of the nonlinear process. Therefore, the HNLFs which are polarization-maintaining is better compared to the HNLFs with random birefringence. However, manufacturing a polarization-maintaining HNLFs with required dispersion and nonlinearities is more expensive and complicated. For parametric amplification, HNLFs with random birefringence are used in a controlled environment in this work.

2.2 Nonlinear effects

There are two classes of nonlinear effects in the optical fiber. The nonlinearities due to Kerr effect make up one class whereas the other class is made of the inelastic scattering due to the vibrational excitation modes of the optical fibers.

2.2.1 Kerr effect

The Scottish physicist John Kerr discovered the Kerr effect in 1875 [21, 22]. The Kerr effect can be defined as change in the refractive index of the medium due to the intensity of the propagating light. The refractive index is not only wavelength-dependent but also depends on the instantaneous intensity of the light. The refractive index dependence on optical intensity is due to the nonlinear polarizability of the medium. The refractive index can be rewritten when taking into account the Kerr effect by introducing an intensity-dependent term as [23]

$$n(\omega, I) = n_0(\omega) + n_2 I, \tag{2.8}$$

where $n_0(\omega)$ is the linear part, n_2 is the nonlinear refractive index and I is the optical intensity associated with the propagating light wave. In optical fibers, the second-order nonlinear effects vanish due to inversion symmetry of the molecules, making the third-order nonlinear effects

dominant. The nonlinear refractive index is

$$n_2 = \frac{3}{4n_0^2\epsilon_0 c}\chi^{(3)}, \tag{2.9}$$

where $\chi^{(3)}$ is the third-order susceptibility, and ϵ_0 is the vacuum permittivity. The nonlinear coefficient (γ) expresses the strength of the nonlinear effects in an optical fiber given by

$$\gamma = \frac{2\pi n_2}{\lambda A_{eff}}, \tag{2.10}$$

where A_{eff} is the effective mode area. The effective mode area corresponds to the confinement of the propagating optical field. The nonlinear coefficient includes the effect of the field distribution with A_{eff}. For the SSMF, the nonlinear coefficient (γ) is about 1.3 (W km)$^{-1}$. In the case of the HNLFs used in our experiments, γ is around 10 (W km)$^{-1}$. HNLFs with γ as high as 30 (W km)$^{-1}$ have also been demonstrated [24]. The accumulated nonlinear phase shift during propagation in the optical fiber can be calculated as

$$\phi_{NL}(z) = \gamma \int_0^z P(z')dz'. \tag{2.11}$$

The accumulated nonlinear phase shift over a physical length (L) can also be calculated using the effective length (L_{eff}) as

$$\phi_{NL}(L) = \gamma L_{eff} P(0), \tag{2.12}$$

where

$$L_{eff} = \frac{1}{\alpha}(1 - \exp(-\alpha L), \tag{2.13}$$

where α is the attenuation coefficient in m^{-1} and L is the physical length of the fiber. The effective length can be defined as the length over which a constant power can give the same nonlinear phase shift (ϕ_{NL}) as the total accumulated phase shift over the actual physical length. For a very long SSMF, the effective length is approximately 21 km. In the case of HNLF, being used in nonlinear applications such as parametric amplification, the physical length should be limited to the order of the effective length as increasing the physical length further only increases the accumulated losses and not the nonlinear interaction. For the parametric amplification in our experiments, the typical lengths of the HNLFs were around 600 m.

The main nonlinear effects due to the Kerr nonlinearities are self-phase modulation (SPM), cross-phase modulation (XPM) and four-wave mixing (FWM).

Self-phase modulation

An optical wave can phase modulate itself by inducing a change in the refractive index of the optical fiber. This process is known as SPM. The accumulated nonlinear phase-shift from SPM for a continuous wave (CW) can be calculated as

$$\phi_{NL}^{SPM}(L) = \gamma P L_{eff}, \tag{2.14}$$

where P is the power of the propagating wave. This also shows how useful is the effective length, L_{eff} in defining the strength of nonlinear process. However, the above equation is valid only in cases where the dispersion can be neglected, i.e., for narrowband signals or when operating at the zero-dispersion wavelength (ZDW) of the optical fiber. Therefore, in other cases where dispersion plays a major role, numerical simulations are required in order to study the interplay between dispersion and SPM. SPM causes a frequency chirp in the propagating optical pulses changing the pulse shape through GVD interaction and broadens the optical spectrum [25], acting as one of the major limitations in single-channel fiber-optic transmission systems. The interaction between SPM and dispersion can also lead to an interesting phenomenon known as optical solitons [26, 27] where the dispersive phase shift and the nonlinear phase shift cancels each other. Optical solitons occur when the optical wave propagates in the anomalous dispersion regime ($\beta_2 < 0$) as the nonlinear phase shift is always positive.

Cross-phase modulation

The phase modulation of an optical wave due to a change in the refractive index induced by another co-propagating optical wave is known as the XPM. In case of a CW, the accumulated phase shift due to XPM when both the waves are propagating in the same polarization is

$$\phi_{NL,12}^{XPM}(L) = 2\gamma P_2 L_{eff}, \tag{2.15}$$

where P_2 is the power of the co-propagating wave. The phase shift due to XPM is two times stronger than that from SPM. However, the factor of two reduces if the amount of co-polarization between the waves decreases. For two orthogonally polarized waves, it becomes

$$\phi_{NL,12}^{XPM}(L) = \gamma P_2 L_{eff}, \tag{2.16}$$

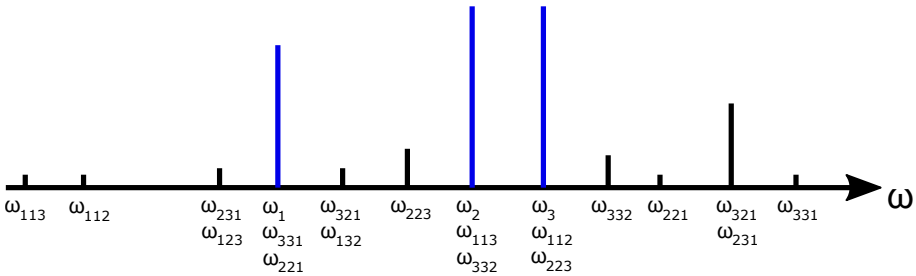

Figure 2.1: Possible FWM components from degenerate and non-degenerate FWM processes.

which has the same strength as SPM. The walk-off due to dispersion also plays a major role when the interacting waves are pulses in case of XPM. The polarization dependence of XPM causes cross-polarization modulation (XpolM) [28], which can be defined as the polarization modulation of a wave due to another wave. We should also take dispersion into account when calculating the strength of XPM and XpolM as in case of SPM. In fiber-optic WDM links with polarization multiplexed signals, apart from SPM, both XPM and XpolM affect the performance of the link [29]. However, concerning this work, only single-polarization signals are considered making XPM the dominating nonlinear effect limiting the throughput.

Four-wave mixing

FWM also known as four-photon mixing involves the nonlinear interaction of four waves and energy transfer between them. Two co-polarised co-propagating waves, E_1 and E_2 with frequencies ω_1 and ω_2 and propagation constants β_1 and β_2 in the optical fiber modulate the refractive index with the intensity beat tone at frequencies $\omega_2 - \omega_1$ as a moving grating with propagation constant, $\beta_2 - \beta_1$. Now, if a third co-polarized co-propagating wave, E_3 is added at the frequency ω_3 with propagation constant β_3, then it will be phase modulated with the frequency $\omega_2 - \omega_1$ generating sidebands at $\omega_4 = \omega_3 \pm (\omega_2 - \omega_1)$ on propagation in the optical fiber. The strength of the process depends on the Bragg condition, $\beta_4 - \beta_3 = \pm(\beta_2 - \beta_1)$ [30]. Similarly, E_2 beats with E_3 and phase modulates E_1, and E_2 is phase modulated by the beat of E_3 and E_1. If the FWM process involves different frequency optical waves, it is said to be non-degenerate and degenerate process involves two waves of the same frequency. With all possible non-degenerate and degenerate FWM

processes, new frequencies are generated at frequencies,

$$\omega_{jkl} = \omega_j + \omega_k - \omega_l, \tag{2.17}$$

For non-degenerate FWM process, $j, k, l \in \{1, 2, 3\},\ j \neq k,\ j \neq l,\ k \neq l$ and in case of degenerate FWM process, $j, k, l \in \{1, 2, 3\},\ j = k \neq l$. Non-degenerate FWM generates six new frequencies. Starting with three waves and only considering first order FWM proceses, both from degenerate and non-degenerate FWM, a total of nine new frequencies are obtained as shown in figure 2.1. Some of the created frequencies will overlap with the original optical waves providing gain while some overlap with each other. Also, few of the created frequencies are stronger known as the idlers. The other weak frequencies are neglected. As in the case above, if all the interacting waves are co-polarized we can call them scalar FWM. In vector FWM, the interacting waves can have different polarizations. Two waves E_1 and E_2 are co-polarized producing a intensity beat tone which phase modulates a cross-polarized wave, E_3 with respect to E_1 and E_2. E_3 scatters energy at $\omega_3 \pm (\omega_2 - \omega_1)$ in the polarization of E_3. In quantum-mechanical interpretation, two photons at frequencies of ω_1 and ω_2 are annihilated to produce two photons at frequencies of ω_3 and ω_4 fulfilling energy $(\omega_1 + \omega_2 = \omega_3 + \omega_4)$ and momentum conservation. The momentum conservation is the quantum-mechanical manifestation of phase matching similar to the Bragg condition determining the efficiency of the FWM. In SSMF, operating in the C-band reduces the effect of FWM due to dispersion. FWM processes in HNLFs can be used to realize parametric amplifiers. These parametric amplifiers are known as fiber-optic parametric amplifiers (FOPA). In this work, FOPAs based on scalar FWM processes are used for amplification. A more complete description of phase matching in FWM and how it affects the parametric amplification will be given in chapter 4.

2.2.2 Inelastic scattering

Inelastic scattering can be defined as the exchange of energy between the optical wave and the vibrational modes of the optical fiber. The two types of inelastic scatterings are Brillouin and Raman scattering.

Brillouin scattering

The electrostriction effect due to an optical field causes Brillouin scattering in the optical fiber inducing acoustic phonons. The energy is

transferred from the propagating optical pump wave to the medium in the form of acoustic vibration producing a downshifted wave called the Stokes wave. This phenomenon can be spontaneous or stimulated, depending on the intensity of the optical wave. Stimulated Brillouin scattering (SBS) was first observed in 1964 [31]. SBS can become dominant if the pump exceeds a certain threshold producing the Stokes wave only in the backward direction relative to the pump. The downshift frequency is dictated by the acoustic phonon which is approximately 10 GHz with a frequency bandwidth of few tens of MHz in silica fiber [23, 32].

Lasers and amplifiers based on SBS have gained attention. Brillouin fiber lasers have been demonstrated [33, 34] with narrow linewidth. SBS based narrowband amplification was used in the regeneration of binary phase-shift keying (BPSK) [35] and quadrature phase-shift keying (QPSK) [36] signals without a phase-locked loop (PLL). It has been demonstrated that Brillouin amplification can also be used as a narrowband filter [37, 38].

The SBS limits the power of the pump wave launched into the optical fiber useful for parametric amplification [39] by inducing nonlinear losses. Several techniques have been developed to increase this limit. The SBS gain is lowered by doping with material like Al_2O_3 [40], however, the dopant increases the loss of the fiber. The SBS travels backward in the optical fiber and can be suppressed by using inline isolators [41]. But, the isolators make the fiber-optic parametric amplifier (FOPA) to be unidirectional and also introduces additional losses. Another way to suppress SBS is to broaden the spectrum of the pump wave more than the SBS spectrum [42]. The pump spectrum is often broadened by phase modulation with radio frequency (RF) tones [43], white noise [44], or pseudo-random bit sequence (PRBS) [45]. Phase modulating the pump transfers the phase modulation to the idler, which degrades the phase-sensitive operation. However using two pumps and counter phase modulating the pump waves, the performance degradation from phase modulation can be removed [45]. SBS can also be reduced by applying a stress gradient [46–48] or a temperature gradient [49, 50] along the fiber, but doing so changes the zero-dispersion wavelength locally affecting the gain and bandwidth of the FOPAs [18]. Fibers tolerant to straining have been developed [51]. These techniques can also be combined to increase the SBS threshold. Strained fibers, along with isolators, have been used in parametric amplifiers to achieve high net gain [52] and is also used in this work. On the other hand, SBS can also enhance the FOPA gain and

bandwidth by changing the signal [53, 54] or pump [55, 56] phase.

Raman scattering

Raman scattering is an inelastic scattering process observed first by C.V. Raman in 1928 [57] for which he was awarded the Nobel prize in Physics in 1930. In the quantum-mechanical description, a photon is annihilated to produce a photon at lower energy or frequency and an optical phonon. The incident light can be described as the pump and the generated downshifted wave as the Stokes wave. Unlike the SBS, the Stokes wave can travel in both the forward and the backward direction. Stimulated Raman scattering (SRS) was discovered in 1962 [58] at high pump power. SRS is a nonlinear process which makes the Stokes wave to multiply quickly by transferring most of the pump energy to the Stokes wave. SRS also depends on the polarizability of the material and is also known as the delayed response of the Kerr effect. In silica fiber, the SRS has a large gain bandwidth whose peak is downshifted about 13.2 THz from the pump wave [23].

Raman amplifiers are interesting as they can perform distributed amplification which is explained in detail in section 3.1.3. Concerning parametric amplification, the Raman effect can be both constructive as well as destructive. SRS can be used to increase the gain and the bandwidth [59]. The crosstalk in FOPAs can be reduced by using SRS [60]. However, SRS can also degrade the performance of the FOPAs [61].

2.3 Numerical modelling

The propagation of light in an optical fiber is modelled using the nonlinear Schrödinger equation (NLSE) [23] as

$$\frac{\partial \tilde{E}}{\partial z} = \underbrace{-i\frac{\beta_2}{2}\frac{\partial^2 \tilde{E}}{\partial t^2} + \frac{\beta_3}{6}\frac{\partial^3 \tilde{E}}{\partial t^3}}_{\text{dispersion}} - \underbrace{\frac{\alpha}{2}\tilde{E}}_{\text{attenuation}} + \underbrace{i\gamma|\tilde{E}|^2\tilde{E},}_{\text{nonlinearity}} \tag{2.18}$$

The envelope of the electric field, $\tilde{E}(z,t)$ is assumed to be slowly varying compared to the carrier wave. The terms have been labelled according to the different physical effects. The effects of Raman and Brillouin scattering have been neglected in (2.18).

2.3.1 Split-step Fourier method

The split-step Fourier method (SSFM) is the most commonly used method for numerical modelling the propagation of light in optical fiber. Though the linear and nonlinear effects acts simultaneously, an approximate solution can be obtained by dividing each step (∂z) in (2.18) into two parts- one that takes care of the linear effect, i.e., dispersion and losses and other for producing the nonlinear rotation. The linear part is given by the differential operator,

$$\hat{D} = -\frac{i\beta_2}{2}\frac{\partial^2}{\partial t^2} + \frac{\beta_3}{6}\frac{\partial^3}{\partial t^3} - \frac{\alpha}{2}, \tag{2.19}$$

while the nonlinear part is given by the nonlinear operator,

$$\hat{N} = i\gamma|\tilde{E}|^2. \tag{2.20}$$

The propagation is then done in steps with size Δz as

$$\tilde{E}(z + \Delta z, t) \approx exp(\Delta z\hat{D})exp(\Delta z\hat{N})\tilde{E}(z, t), \tag{2.21}$$

where the differential operator is evaluated in the frequency domain and the nonlinear operator in the time domain, consecutively. The SSFM is used in this thesis to model the propagation of single- and multi-channel signals for single- and multi-span transmission links.

Chapter 3

Overcoming linear impairments

In this chapter, we will discuss various techniques to overcome the linear impairments in the optical fibers. The fiber loss can be compensated by amplifying the signal with the optical amplifiers, and dispersion can be undone by using dispersion-compensating fibers or modules.

3.1 Optical amplification

In a fiber-optic communication link, the optical fiber attenuates the signal upon propagation which is compensated with optical amplification. However, during amplification, the signal degrades due to the addition of noise by the amplifier. The main requirements for an optical amplifier are to have a high gain and to add a little noise. For WDM systems, one other requirement is to have a broad and flat bandwidth as to not induce any imbalance in power between the channels. In modern communication systems, higher-order modulation formats are targeted to increase spectral efficiency. Therefore, amplifiers should also not add distortions to signals using higher-order modulation formats. Also, the cost and efficiency of optical amplification need to be considered. The optical amplifiers should have low pump power per dB gain. The most common optical amplifier is the EDFA. Other amplifiers such as the semiconductor optical amplifiers (SOA), Raman amplifiers and parametric amplifiers having different gain mechanisms and properties are also of interest. These amplifiers are also known as phase-insensitive amplifiers (PIAs) as the gain is independent of the signal phase. When the signal is

amplified, the amplifier also adds noise known as amplified spontaneous emission (ASE) with a power spectral density [62],

$$S_{ASE} = \eta_{sp} h \nu_0 (G - 1), \tag{3.1}$$

per polarization, where η_{sp} is the spontaneous emission factor, h is the Planck's constant and ν_0 is the frequency of light. The noise figure (NF) is defined as the ratio of the signal-to-noise ratio (SNR) at the input to the SNR at the output of the amplifier [62]. In the high gain regime,

$$NF = \frac{SNR_{in}}{SNR_{out}} \approx 2n_{sp}. \tag{3.2}$$

For PIAs, the spontaneous emission factor is always greater than 1. Therefore, the quantum-limited NF is 3 dB [63]. In practice, the NF usually varies between 4-10 dB in commercial amplifiers.

3.1.1 Erbium-doped fiber amplifiers

EDFAs are the most commercially used optical amplifiers. After its invention in 1986 [8], the EDFAs were commercialised in the mid-1990s which removed the need for signal regeneration, i.e., converting the optical signals to the electrical domain and back to the optical domain. Moreover, EDFAs also support WDM systems. The EDFA has a gain bandwidth of around 40 nm spanning the entire C-band from 1530 nm to 1570 nm. However, it can also be used in the longer 'L'-band from 1570 nm to 1610 nm by increasing the erbium doping concentration [64]. Optical pumping excite the ions to the higher energy state creating a population inversion. The excited ions amplify the signal through the process of stimulated emission. However, spontaneous emission also takes place and gets amplified, adding noise to the amplified signal as ASE. The primary source of noise in EDFAs is the ASE noise. The response time of the EDFAs is slow in the order of milliseconds. Therefore, one can operate the EDFAs in saturation and have no signal distortion or channel crosstalk in WDM systems. i.e., even under saturation, the EDFAs can still serve as a linear amplifier in the bit level. The EDFAs are also polarization-insensitive and have high gain, high gain efficiency and low noise figure. EDFAs with a gain efficiency of 0.1 mW pump power per dB of gain [65] and an NF of 3.1 dB with a gain of 54 dB [66] have been demonstrated.

3.1.2 Semiconductor optical amplifiers

Semiconductor optical amplifiers (SOAs) were developed in 1980 and can have a bandwidth around 50 nm operating from 850 nm to 1600 nm depending on their design. The SOAs are electrically pumped and produces gain through the process of stimulated emission. They are compact and very power efficient. However, there are certain drawbacks. Coupling light from the optical fiber to the SOA and vice versa is inefficient. The lossy input coupling gives us a high black-box NF, and the output coupling leads to losses. SOAs with a gain of 29 dB and noise figure of 7.2 dB have been demonstrated [67]. The nonlinearities in the SOAs can lead to crosstalk in WDM signal amplification distorting the signal, partially due to the picosecond response time [68]. Also, the amplification by SOAs is polarization-dependent. Therefore, SOAs cannot compete with EDFAs but play a vital role in signal processing applications such as all-optical regeneration and wavelength conversion.

3.1.3 Raman Amplifiers

Raman amplifiers exploit the phenomenon of SRS for signal amplification [69]. A strong pump is used to excite the molecules in the medium, and a weak signal is amplified, producing an optical phonon. The gain through SRS depends on the frequency separation between the pump and the signal wave, the medium, the signal and pump polarization and the pump intensity. The maximum gain is obtained when the pump and signal are co-polarized. In silica fiber, the gain is 13.2 THz downshifted from the pump and has a broad bandwidth of 40 THz due to the amorphous nature of silica. The broad gain bandwidth makes Raman amplifier a strong contender for WDM signal amplification outside C-band. The gain efficiency for the Raman amplifiers is low with approx. 10mW pump power per dB gain. The gain starts to build up almost exponentially after some threshold. A Raman amplifier with a gain of 45 dB has been demonstrated [70]. Raman amplifiers can be made polarization-insensitive by scrambling the polarization of the pump. The response time of Raman amplifiers is in the order of picoseconds. Raman amplifiers can be implemented in both lumped and distributed configurations. In the distributed configuration, the signal gain is distributed along the propagating fiber leading to low insertion losses and improved NF. Distributed Raman amplification along with EDFAs have been demonstrated to obtain longer reach [71]. The ASE

noise from spontaneous Raman scattering is the dominant noise source in Raman amplifiers.

Distributed Raman amplification

Ideal distributed Raman amplification provides us with a transparent link, i.e., zero loss across the fiber and a flat power map. Distributed Raman amplification can be implemented in several ways. The simplest way to achieve close to flat power map is to use a single backward pump in the transmission fiber. A local gain is produced in the latter parts of the transmission fiber which alters the power map and improves the link NF. A much flatter power map can be obtained by dividing the span into three segments and backward pumping each of them individually as in paper B. It was possible in the lab, but in reality, might need active elements in the span. However, bi-directional pumping or higher-order Raman schemes can be used instead of the above method to obtain a much flatter power map. The DRA can be modelled by rewriting (2.18),

$$\frac{\partial \tilde{E}}{\partial z} = -i\frac{\beta_2}{2}\frac{\partial^2 \tilde{E}}{\partial t^2} + \frac{\beta_3}{6}\frac{\partial^3 \tilde{E}}{\partial t^3} + \frac{g(z)-\alpha(z)}{2}\tilde{E} + i\gamma|\tilde{E}|^2\tilde{E}, \tag{3.3}$$

where $g(z)$ and $\alpha(z)$ are the local gain and attenuation. DRA with backward pumped Raman can be implemented using the local gain in the amplitude domain with Raman pump power, P_0 as

$$g(z) = \sqrt{g_R \frac{P_0 \exp(-\alpha_p(L-z))}{a_p}}, \tag{3.4}$$

where g_R is the Raman gain coefficient, a_p is the cross-sectional area of the pump in the optical fiber and α_p is the attenuation at the Raman pump wavelength. The net gain from the DRA can be calculated by integrating the square of the local gain over the entire span as

$$G = \exp\left(\int_0^L g_R \frac{P_0 \exp(-\alpha_p(L-z))}{a_p} dz - \alpha L\right), \tag{3.5}$$

whereas the Raman on-off gain, G_R is given by

$$G_R = \exp\left(\int_0^L g_R \frac{P_0 \exp(-\alpha_p(L-z))}{a_p} dz\right). \tag{3.6}$$

Assuming the loss in the pump and signal is same, the link NF with backward pumped DRA from [72] is

$$NF_{DRA,back} = 1 + 2\frac{\eta_{sp}\alpha}{g_R P_0}(G_R - 1). \tag{3.7}$$

For an ideal DRA, where the distributed gain balances the loss at each point in the span, the NF can be further simplified as

$$NF_{DRA,ideal} \approx 10\log(2\alpha_s L + 1) \tag{3.8}$$

where $\exp(\alpha_s L)$ is the net gain needed to counterbalance the span loss and α_s is the loss at the signal wavelength. However, it is difficult to achieve ideal Raman amplification in practise but higher order Raman pumping can provide almost similar performances. Apart from providing better link NF, the symmetric power map from DRA can be useful in mitigation of nonlineairities which will be discussed in chapter 6.

3.1.4 Parametric amplifiers

Parametric amplifiers are based on process of four-wave mixing (FWM). FWM can be defined as the transfer of energy between different frequencies in an elastic manner. i.e., the energy is conserved. Let us inject a strong wave at ω_P called a pump, and a weak wave at ω_S called a signal into the optical fiber. The pump photon is scattered to the signal wave at ω_S and also to a new wave called an idler at $\omega_I = 2\omega_P - \omega_S$. Similarly, the signal photon is scattered to the pump wave at ω_P and a new wave at $2\omega_S - \omega_P$. However, the scattering of the signal photon is negligible compared to the scattering from the pump photon. This process is known as degenerate or single-pumped FWM. The single-pumped FWM amplifies the signal and creates a new wave called the idler. In dual-pumped or non-degenerate FWM, two strong pumps at ω_{P1} and ω_{P2} are used with a weak signal wave at ω_S amplifying the signal wave and producing an idler at $\omega_I = \omega_{P1} + \omega_{P2} - \omega_S$. The degenerate and non-degenerate FWM processes that are used to achieve parametric amplification in optical fibers known as the fiber-optic parametric amplifiers (FOPAs). Therefore, FOPAs are polarization-dependent, and the design of the optical fiber mainly dictates their gain bandwidth. Since the FOPAs are based on the Kerr nonlinearity, their response time is in the order of femtoseconds making them instantaneous. The primary source of noise in parametric amplifiers is the amplified quantum noise (AQN), also known

as the parametric fluorescence or ASE. Parametric amplifiers are the device used for amplification in this work either in phase-insensitive (PI) or phase-sensitive (PS) mode. The PI operation is explained in detail in chapter 4 and the PS in chapter 5.

3.1.5 Amplifier configurations

In optical communications, the optical amplifiers can be used for different purposes. The common amplifier configurations are shown in figure 3.1. An optical amplifier can be placed after the transmitter to increase the signal level before being transmitted known as the booster. The sensitivity can be increased by placing an amplifier before the receiver known as the pre-amplifier. If we have a span followed by a lumped loss and then a lumped amplification as in paper B, the net link NF can be calculated using the Friis formula [73] in linear units,

$$NF_{eq} = NF_{span} + \frac{NF_{loss} - 1}{G_{span}} + \frac{NF_{amp} - 1}{G_{loss}}. \tag{3.9}$$

In long haul fiber-optic communication, the optical amplifiers can be used in between the spans to compensate for the span losses known as the inline amplifier. The optical amplifiers can be placed before or after the transmission span referred to type A or B, respectively, leading to different span NFs. The type A pre-compensates for the fiber loss and type B post-compensates. When using PIAs, the NFs are given as [74],

$$NF^{A}_{PIA-PIA} = 1 + 2N(1 - \frac{1}{G}), \tag{3.10}$$

$$NF^{B}_{PIA-PIA} = 1 + 2NG(1 - \frac{1}{G}), \tag{3.11}$$

where G is the gain in the PIA which is equivalent to the losses in the transmission span, and N is the number of spans.

3.2 Dispersion compensation

Unchirped pulses broaden propagating in an optical fiber. This causes significant limitations in the fiber-optic communication systems. Dispersion compensation can be performed in either optical or electrical domain. In the optical domain, dispersion compensating fiber (DCFs) or dispersion-compensating modules (DCMs) made of chirped fiber-Bragg

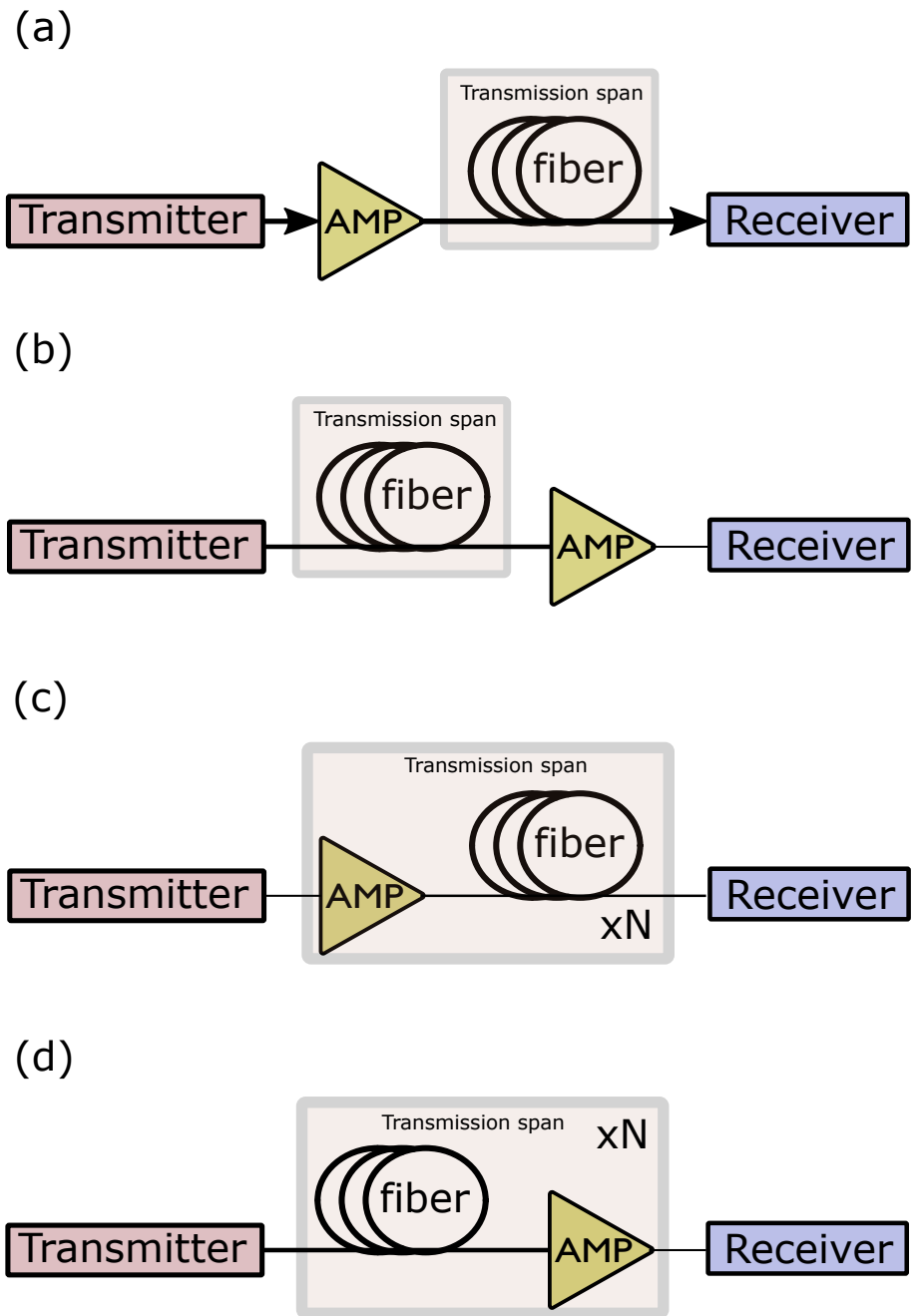

Figure 3.1: Different configurations in which optical amplifiers can be used in a fiber-optic communication link, a) booster amplifier, b) pre-amplifier, c) inline - type A amplifier, d) inline - type B amplifier.

grating (FBG) are used. The dispersion can also be compensated in the electrical domain using the digital signal processing (DSP) with coherent receivers [75].

3.2.1 Dispersion compensating fibers

In order to compensate for the accumulated dispersion and undo the broadening in the SSMF, fibers with negative dispersion ($D < 0$) are used. They are called DCFs, and have very large negative dispersion parameter as well as higher attenuation compared to the SSMF. A few hundred meters to kilometers of DCFs are enough to compensate dispersion over several tens of kilometers of SSMF. In SSMF, the dispersion parameter (D) is about 18 ps/(nm km) and DCFs are designed with dispersion parameter as high as -300 ps/(nm km). The total accumulated dispersion for 80 km of the SSMF is 1440 ps/(nm). The total accumulated dispersion can be compensated with just 4.8 km of DCFs. Due to the high losses involved with the dispersion compensation, the measure of dispersion compensation efficiency is given by a figure of merit (FOM). The FOM is defined as the ratio of the dispersion parameter (D), and the loss per unit DCF length,

$$FOM = \frac{|D|}{\alpha / L_{DCF}}. \tag{3.12}$$

In DCFs, typically FOM is between 150 and 200 ps/(nm dB). But, DCFs with high FOM of 459 ps/(nm dB) has been demonstrated [76]. However, the DCFs have high nonlinearities which can become an important limiting factor in dispersion-managed systems.

3.2.2 Dispersion compensating modules

One other way to compensate for dispersion optically is to use dispersion-compensating modules (DCMs). The absence of nonlinearities, lower loss, negligible latency have made the fiber-Bragg grating (FBG)-based DCMs attractive for dispersion compensation. The FBG-based DCMs may be tunable and can be channelized or continuous in frequency. However, the group-delay ripple in the FBG-based DCMs can limit the performance of the fiber-optic communication link [77]. In this work, the accumulated dispersion in the transmission span is compensated inline for every span using tunable FBG-based DCMs. The tunability of the dispersion settings in the DCMs comes in handy when optimising the dispersion map for nonlinearity mitigation in PSA links.

3.2.3 Compensating dispersion in digital signal processing

The dispersion compensation can be moved to the DSP at the receiver [75, 78] in coherent systems. By using electronic dispersion compensation (EDC), the dispersion compensation in the optical domain can be removed, reducing the loss in the transmission system. The EDC is performed by applying an inverse dispersion transfer function of the link. It can be implemented in both frequency and time domain. For compensating smaller dispersion values, the time domain method is less complex and faster and vice versa. The EDC is performed channel-wise and so is not energy efficient. As the modern transmitters also rely on the digital-to-analog converters (DACs), the EDC can also be performed in the transmitter or the receiver.

Chapter 4

Parametric amplifiers

Parametric amplifiers have been used as pre-amplifier and inline amplifier in this work. In this chapter, we will first solve the coupled-equations for the non-degenerate FWM process explaining the basics behind parametric amplification and then obtain the relation for phase-matching. Similarly, the phase-matching condition is also calculated for the degenerate FWM. Later, the gain bandwidth of the single- and dual-pumped FOPAs are calculated analytically.

4.1 Dual-pumped or non-degenerate FWM

Let us consider a dual-pumped FWM process with two pumps, one at ω_{P1} and ω_{P2}, a signal at ω_S and an idler at ω_I. As we will be dealing with only scalar FOPAs, all waves are assumed to be co-polarized. The total electric field can be written as [23]

$$\begin{aligned}\tilde{E}_{tol}(x,y,z) = \frac{f(x,y)}{2}[&\tilde{E}_{P1}(z)\exp(-i(\omega_{P1}t-\beta(\omega_{P1})z)) \\ &+\tilde{E}_{P2}(z)\exp(-i(\omega_{P2}t-\beta(\omega_{P2})z)) \\ &+\tilde{E}_{S}(z)\exp(-i(\omega_{S}t-\beta(\omega_{S})z)) \\ &+\tilde{E}_{I}(z)\exp(-i(\omega_{I}t-\beta(\omega_{I})z))] + c.c.,\end{aligned} \tag{4.1}$$

where c.c. is the complex conjugate and it is usually omitted in the analysis. $f(x,y)$ represents the transverse mode profile and we assume it to be same for all the waves. Using (2.18), the above expression can be written as four-coupled equations ignoring fiber loss, wavelength dependence on γ, and considering the pumps, signal and idler are CWs or have negligible bandwidth over the pumps, signal and idler bands [23],

$$\frac{d\tilde{E}_{P1}}{dz} = i\gamma(|\tilde{E}_{P1}|^2 + 2|\tilde{E}_{P2}|^2 + 2|\tilde{E}_S|^2 + 2|\tilde{E}_I|^2)\tilde{E}_{P1} + i2\gamma\tilde{E}_S\tilde{E}_I\tilde{E}^*_{P2}\exp(i\Delta\beta z), \tag{4.2}$$

$$\frac{d\tilde{E}_{P2}}{dz} = i\gamma(|\tilde{E}_{P2}|^2 + 2|\tilde{E}_{P1}|^2 + 2|\tilde{E}_S|^2 + 2|\tilde{E}_I|^2)\tilde{E}_{P2} + i2\gamma\tilde{E}_S\tilde{E}_I\tilde{E}^*_{P1}\exp(i\Delta\beta z), \tag{4.3}$$

$$\frac{d\tilde{E}_S}{dz} = i\gamma(|\tilde{E}_S|^2 + 2|\tilde{E}_{P1}|^2 + 2|\tilde{E}_{P2}|^2 + 2|\tilde{E}_I|^2)\tilde{E}_S + i2\gamma\tilde{E}_{P1}\tilde{E}_{P2}\tilde{E}^*_I\exp(-i\Delta\beta z), \tag{4.4}$$

$$\frac{d\tilde{E}_I}{dz} = i\gamma(\underbrace{|\tilde{E}_I|^2}_{\text{SPM}} + \underbrace{2|\tilde{E}_{P1}|^2 + 2|\tilde{E}_{P2}|^2 + 2|\tilde{E}_S|^2}_{\text{XPM}})\tilde{E}_S + i2\gamma\underbrace{\tilde{E}_{P1}\tilde{E}_{P2}\tilde{E}^*_S\exp(-i\Delta\beta z)}_{\text{FWM}}, \tag{4.5}$$

where

$$\Delta\beta = \beta(\omega_S) + \beta(\omega_I) - \beta(\omega_{P1}) - \beta(\omega_{P2}), \tag{4.6}$$

is the linear phase mismatch. On the right hand side of (4.2) to (4.5), the first term corresponds to the SPM-induces phase shifts, second group of terms correspond to the XPM-induced phase-shift, and the last term corresponds to the FWM. The XPM-induced phase-shift is twice that of the SPM-induced phase-shift for co-polarized waves. It is also clear that the FWM depends on $\Delta\beta$ which corresponds to the relative phase between the waves. SPM and XPM depend only on the intensity and do not require phase-matching. These four equations can be used to study most of the parametric processes. Assuming $\tilde{E}(z) = \sqrt{P(z)}\exp(i\phi(z))$, where P is the power and ϕ is the phase of the wave, then (4.2) to (4.5) can be written as [79]

$$\frac{dP_{P1}}{dz} = \frac{dP_{P2}}{dz} = -4\gamma\sqrt{P_{P1}P_{P2}P_SP_I}\sin(\theta), \tag{4.7}$$

$$\frac{dP_S}{dz} = \frac{dP_I}{dz} = 4\gamma\sqrt{P_{P1}P_{P2}P_SP_I}\sin(\theta), \tag{4.8}$$

where

$$\begin{aligned}\frac{d\theta}{dz} &= \Delta\beta + \gamma(P_{P1} + P_{P2} - P_S - P_I) \\ &+2\gamma(\sqrt{\frac{P_{P1}P_{P2}P_S}{P_I}} + \sqrt{\frac{P_{P1}P_{P2}P_I}{P_S}} \\ &-\sqrt{\frac{P_{P1}P_SP_I}{P_{P2}}} - \sqrt{\frac{P_{P2}P_SP_I}{P_{P1}}})\cos(\theta),\end{aligned} \tag{4.9}$$

where $\theta(z) = \Delta\beta z + \phi_{P1}(z) + \phi_{P2}(z) - \phi_S(z) - \phi_I(z)$ describes the relative phase difference between the four involved waves. The first term in (4.9) on the right hand side corresponds to the linear phase shift, second and the third term describes the nonlinear phase shift. From (4.7) to (4.9), by controlling the relative phase, we can dictate the direction of power flow either from the pump to the signal and idler waves where $\theta = \pi/2$ corresponding to parametric amplification or from signal and idler to the pump waves where $\theta = -\pi/2$ for parametric attenuation. This condition is referred to as phase matching for the FWM process. Also it is evident that the power growth is same in the signal and idler with an equal reduction in the two pump powers or vice versa depending on whether $\theta = \pi/2$ or $-\pi/2$ which leads us to the Manley-Rowe relation [80]. If we initially have strong pumps, a weak signal and no idler, the idler will be generated at an infinitesimal propagation distance [81] with $\theta = \pi/2$. Considering phase-matched FWM process that amplifies the signal, $\theta = \pi/2$, the last term on the right hand side of (4.9) becomes zero. Then (4.9) becomes

$$\frac{d\theta}{dz} = \Delta\beta + \gamma(P_{P1} + P_{P2} - P_S - P_I). \tag{4.10}$$

Introducing the phase mismatch parameter, κ and assuming the power of pumps are much higher than the signal and idler waves, we can write the condition to remain phase-matched as

$$\frac{d\theta}{dz} = 0 = \Delta\beta + \gamma(P_{P1} + P_{P2}) \equiv \kappa. \tag{4.11}$$

The coupled equations (4.2) to (4.5) can be solved by assuming undepleted pump waves. Then, the pump fields with pump powers, $P_{P1} = |\tilde{E}_{P1}|^2$ and $P_{P2} = |\tilde{E}_{P2}|^2$ can be written as [82]

$$\tilde{E}_{P1}(z) = \tilde{E}_{P1}(0)\exp[i\gamma(P_{P1} + 2P_{P2})z], \tag{4.12}$$

$$\tilde{E}_{P2}(z) = \tilde{E}_{P2}(0)\exp[i\gamma(P_{P2} + 2P_{P1})z], \tag{4.13}$$

where $\tilde{E}_{P1}(0)$ and $\tilde{E}_{P2}(0)$ corresponds to initial pump fields. In the small-signal regime, the pumps are affected only by the SPM and XPM between them. The signal and idler fields are

$$\tilde{E}_S(z) = [\mu(z)\tilde{E}_S(0) + \nu(z)\tilde{E}_I^*(0)].\exp(-i\frac{1}{2}[\Delta\beta - 3\gamma(P_{P1} + P_{P2})]z), \tag{4.14}$$

$$\tilde{E}_I(z) = [\mu(z)\tilde{E}_I(0) + \nu(z)\tilde{E}_S^*(0)].\exp(-i\frac{1}{2}[\Delta\beta - 3\gamma(P_{P1} + P_{P2})]z). \tag{4.15}$$

For simplicity, the phase terms are often neglected in the (4.14) and (4.15). The μ and ν are the transfer functions defining the input and output relation:

$$\mu(z) = \cosh(gz) + i\frac{\kappa}{2g}\sinh(gz), \tag{4.16}$$

$$\nu(z) = 2i\gamma\frac{\tilde{E}_{P1}(0)\tilde{E}_{P2}(0)}{g}\sinh(gz), \tag{4.17}$$

where $|\mu(z)|^2 - |\nu(z)|^2$ always equal to 1 and g is the parametric gain given as

$$g = \sqrt{4\gamma^2 P_{P1}P_{P2} - (\frac{\kappa}{2})^2}. \tag{4.18}$$

In this analysis, we have considered only four wave interaction. In some cases, there might be a need to consider six-wave interactions involving two pumps, one signal and three idlers for a complete analysis [83]. Moreover, we have assumed small signal regime. At large signal regime, the pumps will be depleted requiring the use of elliptical functions [84].

4.2 Single-pumped or degenerate FWM

For single pump degenerate FWM where the pump fields cannot be distinguished in frequency, the analysis should be carried out with just three waves. Assuming $\omega_{P1} = \omega_{P2} = \omega_P$ and $\Delta\beta = \beta(\omega_S) + \beta(\omega_I) - 2\beta(\omega_P)$, similar to equations (4.7) (4.8) and (4.9) for the dual-pump FWM, the equations for the single-pumped FWM processes are derived as [85]

$$\frac{dP_P}{dz} = -4\gamma\sqrt{P_P^2 P_S P_I}sin(\theta), \tag{4.19}$$

$$\frac{dP_S}{dz} = \frac{dP_I}{dz} = 2\gamma\sqrt{P_P^2 P_S P_I}sin(\theta), \tag{4.20}$$

$$\begin{aligned}\frac{d\theta}{dz} &= \Delta\beta + \gamma(2P_P - P_S - P_I) \\ &+\gamma(\sqrt{\frac{P_P^2 P_S}{P_I}} + \sqrt{\frac{P_P^2 P_I}{P_S}} - 4\sqrt{P_S P_I})cos(\theta),\end{aligned} \tag{4.21}$$

where the relative phase difference, $\theta(z) = \Delta\beta z + 2\phi_P(z) - \phi_S(z) - \phi_I(z)$, and the phase-matching condition can be written as

$$\kappa \equiv \Delta\beta + 2\gamma P_P = 0. \tag{4.22}$$

The parametric gain, μ and ν are [82]

$$g = \sqrt{\gamma^2 P_P^2 - (\frac{\kappa}{2})^2}, \tag{4.23}$$

$$\mu(z) = \cosh(gz) + i\frac{\kappa}{2g}\sinh(gz), \tag{4.24}$$

$$\nu(z) = i\gamma\frac{\tilde{E}_P^2(0)}{g}\sinh(gz). \tag{4.25}$$

4.3 Phase-insensitive amplifier

In case of no idler at the input, from (4.14) and (4.15), the output signal and idler are independent of the phase relation between the interacting waves. They are said to be operating in PI mode know as phase-insensitive amplifiers (PIAs). The phase-insensitive operation is shown in figure 5.2(a). Then, the signal gain for the PIAs is given by,

$$G_S = |\mu(z)|^2, \tag{4.26}$$

which in case of dual-pump PIAs can be written as

$$G_S = 1 + [\frac{2\gamma\sqrt{P_{P1}P_{P2}}}{g}\sinh(gz)]^2, \tag{4.27}$$

and for single-pump PIAs is [85],

$$G_S = 1 + [\frac{\gamma P_P}{g} \sinh(gz)]^2. \tag{4.28}$$

The internally generated idler will have a conversion efficiency given by

$$G_I = |\nu(z)|^2, \tag{4.29}$$

which for the dual-pump PIAs is

$$G_I = [\frac{2\gamma\sqrt{P_{P1}P_{P2}}}{g} \sinh(gz)]^2. \tag{4.30}$$

and in case of the single-pump PIAs [85],

$$G_I = 1 + [\frac{\gamma P_P}{g} \sinh(gz)]^2. \tag{4.31}$$

The generated idler will have a phase, $\phi_I(0) = \phi_S(0) - \Delta\beta z - \phi_{P1}(0) - \phi_{P2}(0)$ and $\phi_I(0) = \phi_S(0) - \Delta\beta z - 2\phi_P(0)$ for the dual- and single-pump PIAs, respectively. Also, the generated idler will be a conjugated copy of the signal which plays an important role in the implementation of modulation format independent phase-sensitive amplifiers as well as in the mitigation of nonlinearities in the transmission link.

4.3.1 Phase-matching

Phase-matching refers to the process of maintaining the relative phase (θ) between the different interacting waves constant during propagation. As the waves propagate, the interacting waves obtain a relative phase-shift from the linear phase mismatch caused by the difference in their propagation constant and from the nonlinear phase shift caused by XPM and SPM. The $\Delta\beta$ on the right hand side of (4.10) and (4.22), corresponds to the linear phase-shift and the last term describes the nonlinear phase-shift. The linear and nonlinear phase-shifts cancel out each other keeping the relative phase constant during propagation known as the perfectly phase-matched condition, providing exponential gain. In the nearly phase-matched condition, the relative phase changes by small amount during propagation still providing a good gain. In case of perfect phase-matching, the signal gain and conversion efficiency become maximum with $\kappa = 0$. For the single-pump PIAs, the maximum gain in

the high gain regime when fulfilling the phase-matching condition can be given by

$$G_S^{max} = G_S^{exp} \approx \frac{\exp(2\gamma P_P z)}{4}, \tag{4.32}$$

where the phase-matching condition becomes

$$\Delta\beta = -2\gamma P_P. \tag{4.33}$$

In case of the dual-pump PIAs, the maximum gain and the phase-matching condition is

$$G_S^{max} = G_S^{exp} \approx \frac{\exp(4\gamma\sqrt{P_{P1}P_{P2}}z)}{4}, \tag{4.34}$$

where the phase-matching condition becomes

$$\Delta\beta = -\gamma(P_{P1} + P_{P2}). \tag{4.35}$$

The gain has a exponential dependence on the nonlinear phase-shift and is known as the exponential gain regime. The other special case is when the linear phase shift becomes zero, i.e., $\Delta\beta = 0$, then for a single-pump PIAs with $\kappa = -2\gamma P_P$, a quadratic dependence on the nonlinear phase-shift is obtained as

$$G_S^{quad} \approx (2\gamma P_P z)^2, \tag{4.36}$$

whereas for the dual-pump PIAs, still a exponential gain is obtained [23].

4.3.2 Gain bandwidth

Let us calculate the gain bandwidth of the single- and dual-pump PIAs. Higher order dispersion parameters above β_4 have been neglected. The third order dispersion parameter does not affect the linear phase mismatch. For the single-pump configuration, the pump wavelength is chosen close to the ZDW to improve phase-matching. The linear phase mismatch can be Taylor expanded around the pump frequency (ω_P) as [23],

$$\begin{aligned} \Delta\beta &= \beta(\omega_S) + \beta(\omega_I) - 2\beta(\omega_P) \\ &\approx \beta_2(\omega_S - \omega_P)^2 + \frac{\beta_4(\omega_S - \omega_P)^4}{12}. \end{aligned} \tag{4.37}$$

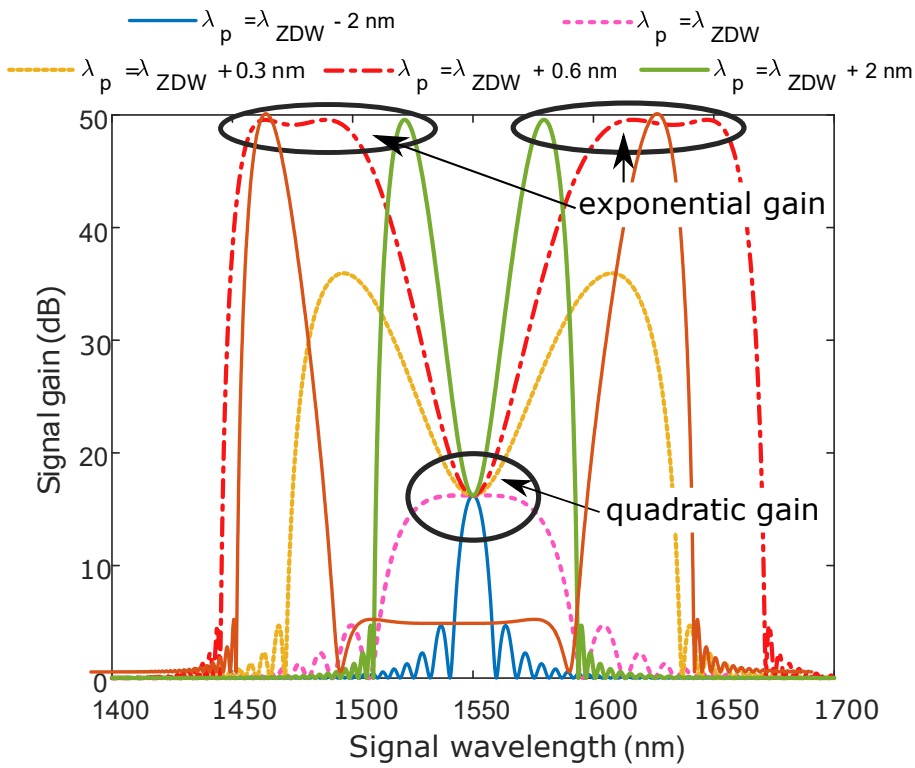

Figure 4.1: Analytically calculated gain bandwidth for a single-pump phase-insensitive amplifier with $\lambda_P = 1550$ nm, $z = 500$ m, $S = 0.02$ ps/(nm^2/ km, $\beta_4 = 2.4$ x 10^{-5} ps^4/km, $\gamma = 16$ $(W\ km)^{-1}$ and $P_P = 800$ mW

The gain bandwidth of the single-pump PIA can be plotted with (4.37). Figure 4.1 shows the gain bandwidth for a single-pump PIA with different ZDW which is similar to sweeping the pump wavelength with fixed ZDW. By pumping in the normal dispersion regime ($D < 0$), we obtain a quadratic gain as seen for $\lambda_P = \lambda_{ZDW} - 2nm$. When pumped at the ZDW, we obtain a flat quadratic gain limited by β_4 as shown in $\lambda_P = \lambda_{ZDW}$. As we pump in the anomalous dispersion regime ($D > 0$), the gain increases more than the quadratic gain as seen for $\lambda_P = \lambda_{ZDW} + 0.3nm$, $\lambda_P = \lambda_{ZDW} + 0.6nm$ and $\lambda_P = \lambda_{ZDW} + 2nm$. We obtain exponential gains for $\lambda_P = \lambda_{ZDW} + 0.6nm$ and $\lambda_P = \lambda_{ZDW} + 2nm$. For large values of $\lambda_p - \lambda_{ZDW}$, second-order dispersion, β_2 dominates and the fourth-order dispersion, β_4 is less important. However, when operating close to ZDW where second-order dispersion, β_2, is very small, β_4 becomes dominant as seen for $\lambda_{ZDW} + 0.6nm$. For the dual-pump configuration, the linear phase mismatch can be Taylor expanded around the center frequency $\omega_C = \frac{\omega_{P1}+\omega_{P2}}{2}$ with $\omega_D = \frac{\omega_{P1}-\omega_{P2}}{2}$ as [23],

$$\begin{aligned} \Delta\beta &= \beta(\omega_S) + \beta(\omega_I) - \beta(\omega_{P1}) - \beta(\omega_{P2}) \\ &\approx \beta_2[(\omega_S - \omega_C)^2 - \omega_D^2] + \frac{\beta_4[(\omega_S - \omega_C)^4 - \omega_D^4]}{12}. \end{aligned} \tag{4.38}$$

When the pumps are far apart, the term given by ω_D in (4.38) dominates the entire large bandwidth. The phase matching can be achieved over the entire bandwidth as $\omega_D^2 >> (\omega_S - \omega_C)^2$, when $\beta_2\omega_D^2 + \frac{\beta_4\omega_D^4}{12} \approx \gamma(P_{P1} + P_{P2})$. Therefore, with ω_C close to the ZDW using two pumps far apart, a flat gain can be obtained over the large gain bandwidth. We also compare the gain bandwidth for the single-pump and dual-pump PIAs in figure 4.2. The pumping frequencies are optimized in each case with respect to the ZDW for flat gain bandwidths and we can find that the dual-pump PIAs can have exponential gain even in the center of the gain bandwidth which is not possible in case of the single-pump PIAs. This dual-pump PIA is obtained only with four wave interaction but in reality might need the solution of the six-coupled equations. In our experiments, the single-pump PIAs have been used as the signal bandwidths are not more than 35 GHz. However, it will be advantageous to move to dual-pump PIAs due to their flat gain bandwidth as we are targeting wavelength-division multiplexed (WDM) communication links.

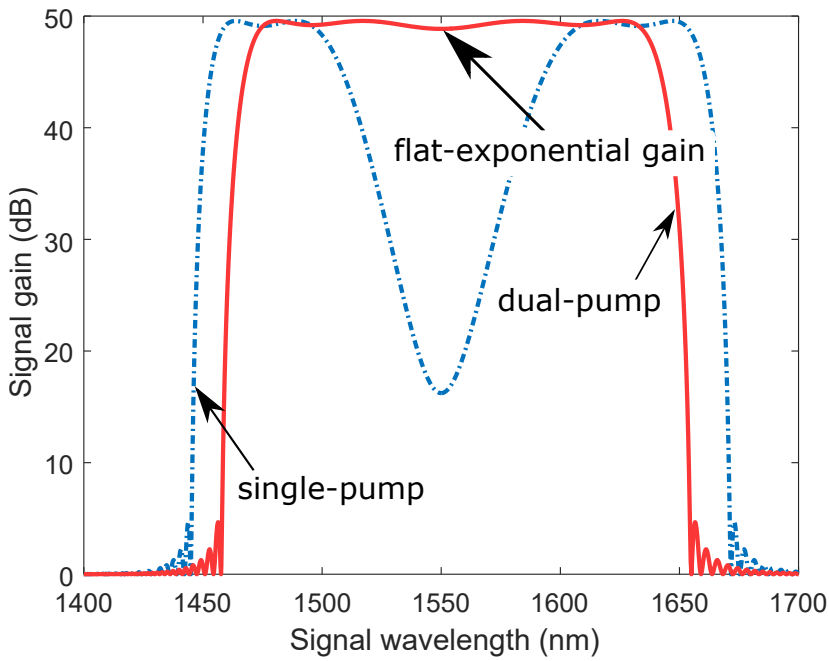

Figure 4.2: Comparison of the analytically calculated maximum gain bandwidth with single and dual-pump phase-insensitive amplifier (PIA) with $\lambda_C = 1550$ nm, $z = 500$ m, $S = 0.02$ ps/(nm^2 km), $\beta_4 = 2.4$ x 10^{-5} ps^4/km, $\gamma = 16$ W^{-1}km^{-1}. For single-pump PIA, $\lambda_C = \lambda_P = \lambda_{ZDW} + 0.6$ nm and $P_P = 800$ mW. For dual-pump PIA, $\lambda_C = \frac{2}{\frac{1}{\lambda_{P1}} + \frac{1}{\lambda_{P2}}} = \lambda_{ZDW} + 0.3$ nm. In both configurations, the pump wavelength were optimized with respect to the zero-dispersion wavelength (ZDW) for maximum gain bandwidth.

4.4 Noise in parametric amplifiers

The main source of noise in parametric amplifiers is the amplified quantum noise [61, 86]. The other noise sources in parametric amplifiers are the pump-transferred noise (PTN) [86] and the Raman scattering [87]. High power pumps are required in the parametric amplification. Therefore, the pump wave is amplified using the EDFA. The in-band noise added by the EDFA at the pump frequency cannot be filtered and causes pump fluctuations which are then transferred as the in-band noise to the signal and idler frequencies through the process of FWM. The performance degradation due to PTN have been studied in PIAs [61, 86]. In practice, it is difficult to achieve the 3 dB quantum-limited noise figure in FOPAs mainly due to Raman scattering. However, under the limit imposed by Raman scattering, the best noise figure demonstrated in phase-insensitive operation is 3.4 dB [87].

Chapter 5

Phase-sensitive amplifiers

In the PIAs, we assumed there is no idler at the input. If we have an idler wave at the input, for single-pump FWM process according to (4.16) and (4.17), and for dual-pump FWM process with (4.24) and (4.25), the output signal and idler depends on the phase relation between the interacting waves known as the phase-sensitive amplifier (PSA). Depending on the number of signal and idler frequencies, and the pumping schemes, there are four popular PSA schemes as shown in figure 5.1. In the first two schemes, the signal and idler have the same frequency known as the one-mode PSAs. The two-mode PSAs are the last two schemes with two different signal and idler frequencies. There is also a four-mode PSA with four different signal and idlers frequencies but is outside the scope of this thesis. The one- and two-mode PSAs will be discussed in detail in the next sections. Later, the two-mode PSA is implemented with the copier-PSA.

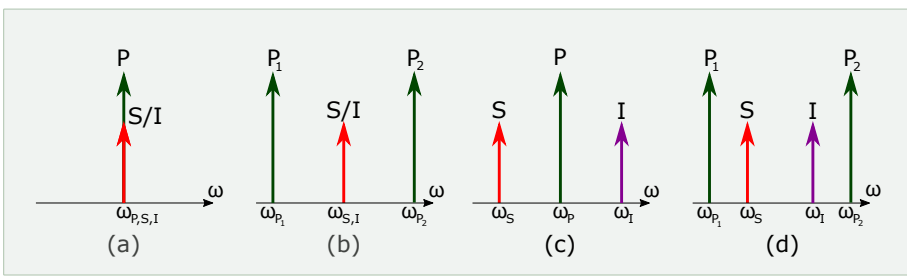

Figure 5.1: PSA scheme based on (a) fully-degenerate FWM, (b) signal-degenerate FWM, (c) pump-degenerate FWM, and (d) non-degenerate FWM.

5.1 One-mode phase-sensitive amplifiers

The fully-degenerate and signal-degenerate PSAs have only one signal and idler frequency to be known as the one-mode phase-sensitive amplifiers. In the fully-degenerate PSA as shown in figure 5.1 (a), the pump, signal and idler lie on the same frequency. i.e., $\omega_P = \omega_S = \omega_I$. Therefore, a Sagnac interferometer [88,89] is required to implement fully-degenerate PSAs. The signal-degenerate PSA is shown in figure 5.1 (b). It consists of two pumps at ω_{P1} and ω_{P2} with the signal and idler at the same frequency ($\omega_S = \omega_I$). The wave frequencies are related by $2\omega_S = 2\omega_I = \omega_{P1} + \omega_{P2}$. The input-output relation for the one-mode phase-sensitive amplifier is given by [82, 88],

$$\tilde{E}_S(z) = \mu(z)\tilde{E}_S(0) + \nu(z)\tilde{E}_S^*(0), \tag{5.1}$$

where $\mu(z)$ and $\nu(z)$ can be calculated from the nonlinear phase-shift [90] in case of the fully degenerate PSA. The fully degenerate PSA has only quadratic dependence of the nonlinear phase shift compared to the maximum exponential dependence in the other schemes. For the signal degenerate PSA, $\mu(z)$ and $\nu(z)$ is given in 4.16 and 4.17, respectively. The signal gain can be calculated as

$$G_S = \frac{|\tilde{E}_S(z)|^2}{|\tilde{E}_S(0)|^2} = |\mu(z)|^2 + |\mu(z)|^2 + 2|\mu(z)||\nu(z)|\cos(\phi(z)), \tag{5.2}$$

where the relative phase, $\phi(z) = 2\phi_S(z)$. In the one-mode PSA, one signal quadrature will be amplified while attenuating the other quadrature, producing a squeezed output signal as shown in figure 5.2 (b).

5.2 Two-mode phase-sensitive amplifiers

Two-mode phase-sensitive amplifiers can be implemented using the pump degenerate scheme as shown in figure 5.1 (c) and the non-degenerate scheme as shown in figure 5.1 (d). The input-output relation for the two-mode PSAs can be obtained using the signal and idler from (4.14) and (4.15) as shown below [91],

$$\tilde{E}_S(z) = \mu(z)\tilde{E}_S(0) + \nu(z)\tilde{E}_I^*(0), \tag{5.3}$$

$$\tilde{E}_I(z) = \mu(z)\tilde{E}_I(0) + \nu(z)\tilde{E}_S^*(0). \tag{5.4}$$

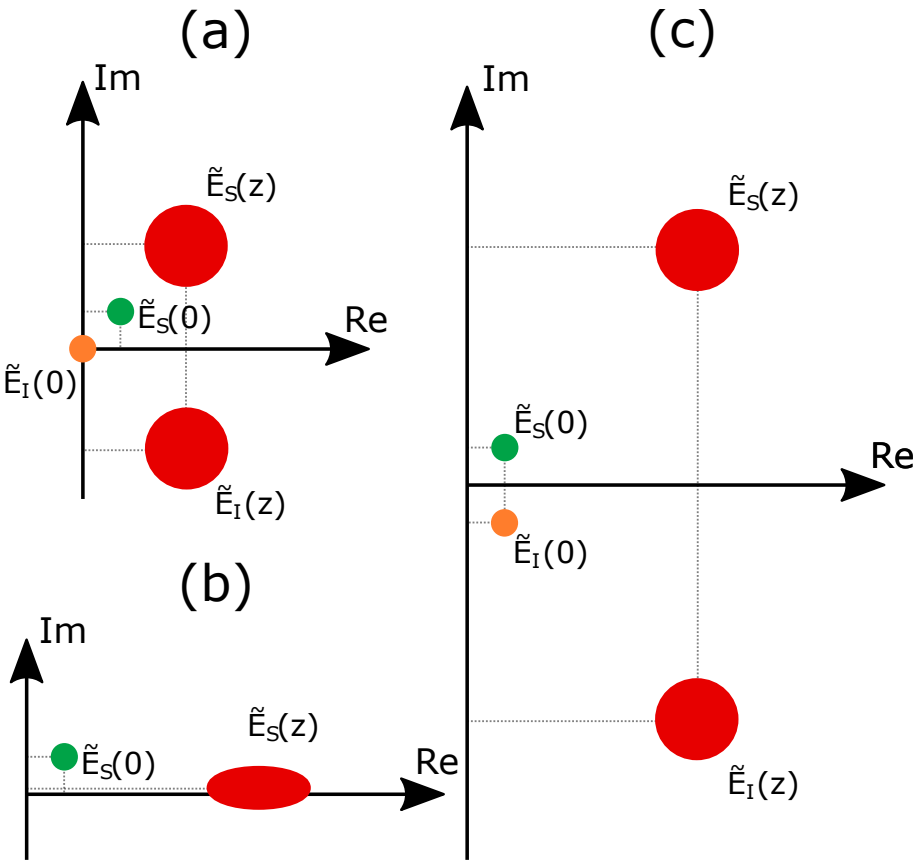

Figure 5.2: Amplification in the high-gain regime with (a) PIA (b) one-mode PSA (c) two-mode PSA, where $\tilde{E}_S(0)$ and $\tilde{E}_I(0)$ are the input signal and idler waves, respectively. The signal and idler output is given by $\tilde{E}_S(z)$ and $\tilde{E}_I(z)$, respectively. The gain in PSA is four times equal to the gain in PIA.

For the pump-degenerate PSA, the signal, pump and idler frequencies are related as $2\omega_P = \omega_S + \omega_I$, and the $\mu(z)$ and $\nu(z)$ are given in (4.24) and (4.25), respectively. In case of the non-degenerate PSA, the relation between the pump, signal and idler frequencies are given by $\omega_{P1} + \omega_{P2} = \omega_S + \omega_I$ and the (4.16) and (4.17) correspond to the $\mu(z)$ and $\nu(z)$ values. Assuming, the idler has the same power as the signal giving the maximum phase interaction at high gain, the gain is given as

$$G_S = \frac{|\tilde{E}_S(z)|^2}{|\tilde{E}_S(0)|^2} = |\mu(z)|^2 + |\nu(z)|^2 + 2|\mu(z)||\nu(z)|\cos(\phi(z)), \tag{5.5}$$

where $\phi(z) = \phi_S(z) + \phi_I(z)$. When we have an idler which is the conjugated copy of the signal with equal powers and phase relation, $\phi_I(z) = -\phi_S(z)$, the maximum gain is given by

$$G_S^{max} = \frac{|\tilde{E}_S(z)|^2}{|\tilde{E}_S(0)|^2} = |\mu(z)|^2 + |\nu(z)|^2 + 2|\mu(z)||\nu(z)| = (|\mu(z)| + |\nu(z)|)^2. \tag{5.6}$$

At the high regime regime where $\mu(z) \approx \nu(z)$, the maximum phase-sensitive gain is equal to the four times the gain of the phase-insensitive amplifier (4.26) as shown in figure. 5.2 (c).

The one-mode PSA is capable of amplifying only pulse-amplitude modulation (PAM). In the two-mode PSA, the idler being the conjugated copy of the signal, any modulation format can be amplified. From, now we restrict our analysis and discussion to the two-mode PSAs using pump-degenerate and fully-degenerate schemes. In our experiments, two-mode PSA has been used with the pump-degenerate scheme. However, fully-degenerate PSAs will be the better scheme for WDM applications due to the flatter gain bandwidth.

5.3 Noise in phase-sensitive amplifiers

Until now, we have excluded the noise produced during amplification. n_S and n_I are the vacuum noise at the signal and idler frequencies, respectively, having a complex Gaussian distribution with $< n_{S/I} >= 0$, $< n_{S/I}^2 >= 0$ and $< |n_{S/I}|^2 >= \frac{hf_{S/I}}{2}$. Then, for the two mode PSA in both the pump-degenerate and fully-degenerate schemes, the equations 5.3 and 5.4 can be written as [91]

$$\tilde{E}_S(z) = \mu(z)[\tilde{E}_S(0) + n_S(0)] + \nu(z)[\tilde{E}_I^*(0) + n_I^*(0)], \tag{5.7}$$

$$\tilde{E}_I(z) = \mu(z)[\tilde{E}_I(0) + n_I(0)] + \nu(z)[\tilde{E}_S^*(0) + n_S^*(0)]. \quad (5.8)$$

When the input signal is shot-noise limited and no idler is present, in the PIAs, the quantum-limited noise figure is 3 dB [86]. The generated idler is the phase-conjugated copy of the signal. The idler noise will also be the phase-conjugated copy of the signal noise. In the high gain regime, the noise figure of the idler can also be deduced as 3 dB. Unless the receiver is thermally limited, detecting both the signal and idler does not increase the SNR.

In the case of the PSA, when the signal and idler waves are shot-noise limited, the noise remains the same. In the high gain regime, the gain of the PSA is four times the gain of the PIA. Therefore, the noise figure becomes -3 dB, considering only the signal. But if we take into account that both the signal and idler waves are present at the input, then the sum of signal and idler noise figures is 0 dB [30]. Only in amplifiers where the signal gain depends on the input wave phases, 0 dB noise figure can be achieved. The signal-degenerate PSA has a quantum-limited noise figure of 0 dB. In the four-mode PSAs, taking only the signal into account, the noise figure is -6 dB. The sum of the signal and idlers noise figure is 0 dB [92]. Similar to PIAs, the PTN [93] and Raman scattering limit the noise performance in PSAs. PSAs with a low noise figure of 1.1 dB have been demonstrated [11].

5.4 Copier-PSA implementation

A modulation format-independent and multi-channel compatible PSA can be implemented with both pump-degenerate and fully-degenerate schemes using the copier-PSA with two HNLFs. The first HNLF is used as a phase-insensitive amplifier or a copier to obtain the three or four frequency- and phase-locked waves. The copier produces an idler which is the conjugated copy of the signal at $\omega_I = 2\omega_P - \omega_S$ for the pump-degenerate scheme and $\omega_I = \omega_{P1} + \omega_{P2} - \omega_S$ for the fully-degenerate scheme. These waves are used in the second HNLF called the PSA to achieve phase-sensitive amplification. For a single span transmission with the span in between the two HNLFs, PSA can act as a pre-amplifier. A copier-PSA implementation using PSA as a pre-amplifier has been demonstrated in paper D for a WDM system to study cross-phase modulation mitigation. The copier-PSA can also be implemented in multi-span, then operating as inline amplifiers as discussed in section 3.1.5. The copier is followed by many sections consisting of the span and PSA.

In papers A-C, PSA is used as an inline amplifier with a copier-PSA implementation to study nonlinearity mitigation.

A shot-noise limited signal is launched with high power pump wave(s) into the copier which produces the idler through FWM. The uncorrelated noise at signal and idler frequencies will add incoherently during the phase-insensitive process in the copier leading to correlated noises in the signal and idler. The signal and idler are attenuated to add uncorrelated vacuum noise and attenuate the correlated noise [91, 94]. The uncorrelated vacuum noise at the signal and idler frequencies, along with the three or four frequency and phase-locked signal, idler and pump wave(s) provide a 6 dB higher SNR compared to using a PIA. By using six frequency and phase-locked signal, idlers and pump waves, a 9 dB higher SNR improvement can be obtained with respect to the PIA. However, if the correlated amplifier noise is not completely attenuated and the noise is not completely uncorrelated, then the advantage decreases [95, 96].

A detailed description is given in figure 5.3. The waves at the output of the copier exactly fulfil the conditions for perfect phase-sensitive operation. Perfect phase-sensitive operation requires the synchronization in time, alignment in polarization and stabilization in the relative phase of the waves. The pump used in the parametric amplifiers should have more than 65 dB OSNR to avoid the noise transfer from pump to signal [97]. In fiber-optic communication system, the loss is caused by the optical transmission fiber producing the uncorrelated vacuum noise. But, the optical fiber also changes the properties of the waves. Therefore, the impact of the transmission span should be undone to obtain perfect phase-sensitive operation. The DCMs is used to compensate for the cumulative chromatic dispersion in the transmission link. Two channelized tunable FBG-based DCMs slope-matched to the transmission fiber are used, one before- and after- the transmission span to apply the required dispersion compensation. The need for two DCMs will be discussed in chapter 6. In order to obtain a high OSNR pump wave(s), the pump(s) need to be separated from the signal and idler. As the DCMs are channelized, delay tuning is used to temporally synchronize the signal and idler waves. The PMD in the transmission link can be compensated by aligning the polarization of the signal and idler. As the pump wave is split from the signal and idler waves and propagated in different fiber, thermal drifts and acoustic vibrations can lead to relative phase drifts. A PLL is used to compensate for the phase drifts with a small fraction of the PSA output as feedback. The weak pump is then recovered

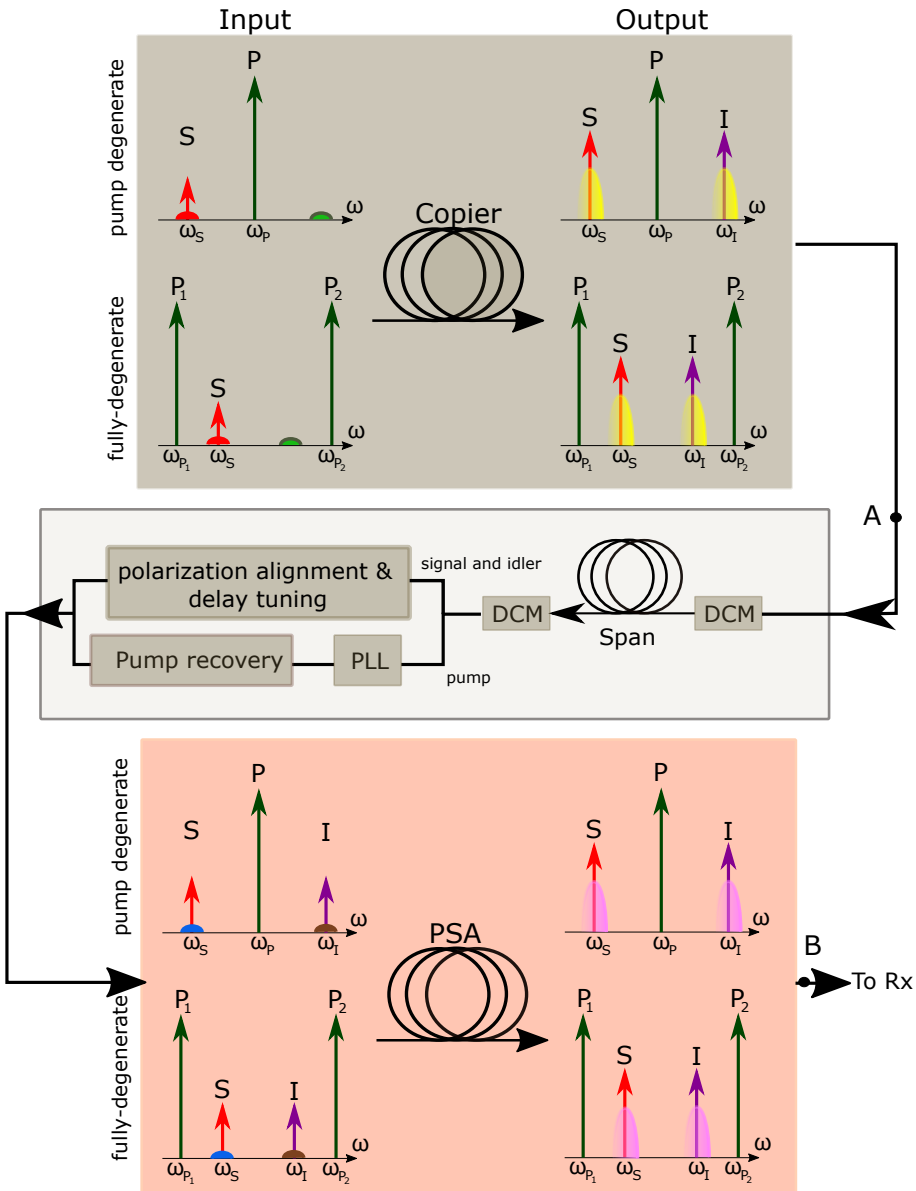

Figure 5.3: Copier-PSA implementation using pump-degenerate and fully-degenerate FWM.

using optical-injection locking (OIL). OIL is a technique in which the phase of the injected laser within a certain bandwidth called the locking bandwidth is transferred to the output high power wave suppressing the amplitude noise. OIL at low injected power of -65 dBm has been demonstrated [98].

The copier-PSA implementation is the most preferred in transmission experiments due to its WDM compatibility and modulation format independency [99]. For a PSA-amplified multi-span link, the section between A and B in the figure 5.3 has to be repeated for each transmission span.

5.4.1 Link noise figure

For the single-span link, in the high-gain regime, assuming idler as a transparent internal mode of the copier-PSA link, with 0 dB net link gain and large loss between the copier and the PSA, the noise figure is given as [11],

$$NF_{copier-PSA} \approx \frac{G}{2}. \tag{5.9}$$

Similarly, for two cascaded PIAs sandwiching a lossy transmission link [11],

$$NF_{PIA-PIA} \approx 2G. \tag{5.10}$$

Comparing (5.9) and (5.10), a 6 dB advantage in SNR can be seen for copier-PSA system compared to the PIA-PIA system, where G corresponds to the gain in the last amplifier. For the multi-span link consisting of N spans, the PSA can be used as inline amplifier in two configurations namely type A and type B as shown in section 3.1.5 using copier-PSA. The noise figure is given by [91],

$$NF^{A}_{copier-PSA} \approx \frac{5}{2} + \frac{N}{2}, \tag{5.11}$$

$$NF^{B}_{copier-PSA} \approx \frac{3G}{2} + \frac{NG}{2}, \tag{5.12}$$

where G is the inline amplifier gain which is equal to the transmission span losses. From (5.11), (5.12), (3.10) and (3.11), in many number of spans ($N >> 1$), with high gain ($G >> 1$), a 6 dB SNR improvement in obtained for both the types of inline amplification using copier-PSA compared to PIA-PIA.

Chapter 6

Overcoming nonlinear impairments

In fiber-optic communication links, the loss incurred by the signal on propagation is overcome by using optical amplifiers. However, during the process of amplification, noise is also added to the signal, limiting the reach or throughput. To increase the reach or throughput, optical power can be increased. However, increasing the optical power of the signal causes distortions due to the Kerr nonlinearities in the optical fiber. The fiber nonlinearities are the other major limiting factor apart from the added amplifier noise [100–103]. These distortions can be caused due to intra-channel effects or inter-channel effects [100]. The nonlinear beating within the signal band causes the intra-channel effects which includes the signal-signal beating leading to SPM and signal-noise beating giving rise to the nonlinear phase noise (NLPN) [104]. The intra-channel effects are the feature of single-channel transmission system. The inter-channel effect is caused by the interaction between the neighbouring signal bands where signal-signal beating leads to XPM or FWM and signal-noise beating results in NPN. The WDM transmission systems are affected by the inter-channel effects due to the Kerr nonlinearites.

The distortions caused by the Kerr effect in the optical fiber can be compensated either optically or digitally [105] after detection. All-optical nonlinearity mitigation techniques include mid-span spectral inversion or optical phase conjugation (OPC) [12], phase-conjugated twin waves (PCTWs) [13], and copier-PSA [106]. Digital signal processing (DSP) techniques like digital back-propagation (DBP) [14] and Volterra based nonlinear equalizers [107] are also commonly used to mitigate Kerr

nonlinearities.

6.1 Nonlinearity mitigation using DSP

In DBP, the detected signal is propagated numerically backwards in DSP with the knowledge of the actual fiber parameters like loss, nonlinear coefficient and dispersion parameter to compensate simultaneously for dispersion and nonlinearities. As the bandwidth of the optical signals increases, the numerical computations becomes more complex [14] and all the channels need to be detected simultaneously in a WDM scenario. Similar to DBP, Volterra based nonlinear equalizer also requires complex computations. A Volterra series can be used to represent the transfer function of the optical fiber in the frequency domain with Volterra kernels. The signal after propagation in the optical fiber is given by as [15]

$$\tilde{E}_S(\omega,z)=\sum_{n=1}^{\infty}\int .....\int K_n(\omega_1,.,\omega_{n-1},\omega-\omega_1+\omega_2-.....\pm\omega_{n-1},z) \times\tilde{E}_S(\omega_1,0)....\tilde{E}_S(\omega_{n-1},0) \times\tilde{E}_S(\omega-\omega_1+\omega_2-.....\pm\omega_{n-1})d\omega_1....d\omega_{n-1}. \tag{6.1}$$

The n^{th}-order Volterra Kernel is given by K_n. The first order linear kernel corresponds to the linear transfer function, and the higher-order kernels are related to the nonlinear response. The even order kernels can be neglected as there are no even-order nonlinearities in fiber due to inversion symmetry. Including the higher-order Kernels increases the computational complexity as well as the accuracy. The closed-form approximation to obtain the link transfer function can be used to apply an inverse filter to compensate for the linear dispersion and fiber nonlinearity known as Volterra nonlinear equalizer (VNLE). Less complex VNLE with just the first- and third-order kernels have been demonstrated to mitigate nonlinearities [108]. In general, a third-order VNLE for N spans with length, L, and considering only second-order dispersion is [105]

$$\tilde{E}_S(\omega,z)\approx K_1(\omega,z)\tilde{E}_S(\omega,z) +\Gamma\iint F(\Delta\Omega)K_3(\Delta\Omega,z)\tilde{E}_S(\omega_1,z)\tilde{E}_S^*(\omega_2,z)\tilde{E}_S(\omega-\omega_1+\omega_2,z)d\omega_1 d\omega_2, \tag{6.2}$$

where K_1 is the first-order Kernel:

$$K_1(\omega, z) = \exp(\frac{\alpha L}{2} - i\frac{\beta_2 \omega^2}{2} z], \tag{6.3}$$

K_3 is the third-order Kernel:

$$K_3(\Delta\Omega, z) = \frac{1 - \exp[(\alpha - i\beta_2 \Delta\Omega)z]}{-\alpha + i\beta_2 \Delta\Omega}, \tag{6.4}$$

$F(\Delta\Omega)$ describes the phased-array effect which is how the nonlinear distortions adds over several spans [108]:

$$F(\Delta\Omega) = \exp(i\frac{\beta_2 \Delta\Omega(N-1)L}{2})\frac{\sin(\frac{\beta_2 \Delta\Omega NL}{2})}{\sin(\frac{\beta_2 \Delta\Omega L}{2})}, \tag{6.5}$$

Γ is the frequency-dependent nonlinear term:

$$\Gamma(\omega, z) = -i\gamma K_1(\omega, z), \tag{6.6}$$

and $\Delta\Omega = (\omega_1 - \omega)(\omega_1 - \omega_2)$. Usually, the losses are compensated inline every span except the last span. Therefore, the linear Kernel, K_1, in the VNLE compensates for the whole dispersion in the transmission link and loss only for the last span.

6.2 All optical nonlinearity mitigation

In OPC, the signal is phase conjugated at the mid-stage of the link. Assuming only second-order dispersion, the dispersion and nonlinearities from the first half of the link can be reversed in the second half after phase conjugation. For effective compensation, the link power map should be symmetric around the mid-stage where the optical phase conjugation happens. By transmitting the signal and phase-conjugated copy of the signal, and performing the coherent superposition of them in DSP after detection, the nonlinearities can be mitigated in PCTWs, This phase-conjugated copy of the signal can be in orthogonal polarization [13], frequencies [109], time [110], and space [111]. Another technique which uses the conjugated copy of the signal is the copier-PSA. As discussed before, the copier generates the conjugated copy of the signal called the idler and two the waves along with the pump are propagated in the transmission link. They experience correlated distortions due to the Kerr

nonlinearities in the optical fiber and are coherently added in the PSA, enabling nonlinearity mitigation and low noise amplification. For both the PCTW and copier-PSA, efficient nonlinearity mitigation requires a symmetric power map with an asymmetric dispersion map. The two tunable dispersion compensation modules in the copier-PSA implementation were used to apply pre- and post-dispersion compensation.

Let us start with a single span link, the input signal to the transmission link is $\tilde{E}_S(t,0)$ and therefore, the idler is the conjugated copy of the signal given by $\tilde{E}_I(t,0) = i\tilde{E}_S^*(t,0)$. Assuming the optical fiber as weakly nonlinear medium and the nonlinear distortions very small compared to the signal, the nonlinear distortions can be modelled as small perturbation to the linear solution using the perturbation theory [112]. Then, the signal and idler after propagation is given as

$$\tilde{E}_S(t,z) = [\tilde{E}_s(t,0) + \delta_{NL,S}(t,z)] \exp(-\frac{\alpha}{2}z + i\frac{\beta_2\omega^2}{2}z), \tag{6.7}$$

$$\tilde{E}_I(t,z) = [\tilde{E}_I(t,0) + \delta_{NL,I}(t,z)] \exp(-\frac{\alpha}{2}z + i\frac{\beta_2\omega^2}{2}z). \tag{6.8}$$

In the copier-PSA link, the dispersion is compensated optically as discussed in section 5.4 for proper PS operation. Therefore, the signal and idler input to the PSA can be written as

$$\tilde{E}_{S,in}(t,z) = [\tilde{E}_S(t,0) + \delta_{NL,S}(t,z)] \exp(-\frac{\alpha}{2}), \tag{6.9}$$

$$\tilde{E}_{I,in}(t,z) = [\tilde{E}_I(t,0) + \delta_{NL,I}(t,z)] \exp(-\frac{\alpha}{2}). \tag{6.10}$$

Assuming that the losses in the link are compensated by PSA with $2|\mu| = 2|\nu| = \exp(\frac{\alpha}{2})$. From (5.3), the signal at the PSA output is

$$\tilde{E}_{S,out}(t,z) = \mu\tilde{E}_{S,in}(t,z) + \nu\tilde{E}_{I,in}^*(t,z), \tag{6.11}$$

$$\tilde{E}_{S,out}(t,z) = 0.5[\tilde{E}_S(t,0) + \delta_{NL,S}(t,z)] + i0.5[\tilde{E}_I(t,0) + \delta_{NL,I}(t,z)]^*, \tag{6.12}$$

$$\tilde{E}_{S,out}(t,z) = 0.5[\tilde{E}_S(t,0) + \delta_{NL,S}(t,z)] + i0.5[(i\tilde{E}_S^*(t,0)) + \delta_{NL,I}(t,z)]^*, \tag{6.13}$$

$$\tilde{E}_{S,out}(t,z) = 0.5[\tilde{E}_S(t,0) + \delta_{NL,S}(t,z) + \tilde{E}_S(t,0) + \delta_{NL,I}^*(t,z)], \tag{6.14}$$

$$\tilde{E}_{S,out}(t,z) = \tilde{E}_S(t,0) + \delta_{NL,res}, \tag{6.15}$$

where $\delta_{NL,res}$ is the residual nonlinear distortion after the nonlinear compensation in the PSA:

$$\delta_{NL,res} = 0.5[\delta_{NL,S}(t,z) + \delta^*_{NL,I}(t,z)]. \tag{6.16}$$

In the frequency domain, from the perturbation theory the nonlinear distortion in the signal can be calculated by summing the possible FWM products between spectral components at ω_1, ω_2 and $\omega_3 = \omega - \omega_1 + \omega_2$ under the influence of the link transfer function as [112],

$$\begin{aligned}\delta_{NL,S}(\omega, L) = i\gamma \iint \eta_S(\Delta\Omega, L)\tilde{E}_S(\omega_1, 0)\tilde{E}^*_S(\omega_2, 0) \\ \tilde{E}_S(\omega - \omega_1 + \omega_2, 0)d\omega_1 d\omega_2,\end{aligned} \tag{6.17}$$

where $\tilde{E}(\omega)$ is the Fourier transform of $\tilde{E}(t)$ and $\eta_S(\Delta\Omega, L)$ is the link transfer function for the signal:

$$\eta_S(\Delta\Omega, L) = \int_0^L \exp[G(z) + j\Delta\Omega D(z)]dz, \tag{6.18}$$

where $G(z)$ describes the evolution of the signal amplitude and $G(z)$ shows how the dispersion is accumulated along the link, i.e., the dispersion map.

Using the Fourier transform relation, $\tilde{x}(t) \longleftrightarrow \tilde{X}^*(-\omega)$, we have $i\delta^*_{NL,I}(t, L) \longleftrightarrow i\delta^*_{NL,I}(-\omega, L)$. From (6.17), the nonlinear distortion in the idler can be calculated as

$$\begin{aligned}i\delta^*_{NL,I}(-\omega, L) = i[i\gamma \iint \eta_I((\omega_1 + \omega)(\omega_1 - \omega_2), L)\tilde{E}_I(\omega_1, 0) \\ \tilde{E}^*_I(\omega_2, 0)\tilde{E}_I(-\omega - \omega_1 + \omega_2, 0)d\omega_1 d\omega_2]^*,\end{aligned} \tag{6.19}$$

$$\begin{aligned}i\delta^*_{NL,I}(-\omega, L) = \gamma \iint \eta^*_I((\omega_1 + \omega)(\omega_1 - \omega_2), L)\tilde{E}^*_I(\omega_1, 0) \\ \tilde{E}_I(\omega_2, 0)\tilde{E}^*_I(-\omega - \omega_1 + \omega_2, 0)d\omega_1 d\omega_2.\end{aligned} \tag{6.20}$$

Substituting $\tilde{E}_I(\omega, 0) = i\tilde{E}^*_S(-\omega, 0)$ in the above equation,

$$\begin{aligned}i\delta^*_{NL,I}(-\omega, L) = \gamma \iint \eta^*_I((\omega_1 + \omega)(\omega_1 - \omega_2), L)(i\tilde{E}^*_S(-\omega_1, 0))^* \\ (i\tilde{E}^*_S(-\omega_2, 0))(i\tilde{E}^*_S(\omega + \omega_1 - \omega_2, 0))^* d\omega_1 d\omega_2,\end{aligned} \tag{6.21}$$

$$\begin{aligned}i\delta^*_{NL,I}(-\omega, L) = -i\gamma \iint \eta^*_I((\omega_1 + \omega)(\omega_1 - \omega_2), L)\tilde{E}_S(-\omega_1, 0) \\ \tilde{E}^*_S(-\omega_2, 0)\tilde{E}_S(\omega + \omega_1 - \omega_2, 0)d\omega_1 d\omega_2,\end{aligned} \tag{6.22}$$

Replacing $\omega_{1,2} \longleftrightarrow -\omega_{1,2}$,

$$i\delta^*_{NL,I}(-\omega, L) = -i\gamma \iint \eta^*_I(\Delta\Omega, L)\tilde{E}_S(\omega_1, 0)\tilde{E}^*_S(\omega_2, 0) \tilde{E}_S(\omega - \omega_1 + \omega_2, 0)d\omega_1 d\omega_2. \tag{6.23}$$

Substituting (6.17) and (6.23) in (6.16),

$$\delta_{NL,res} = 0.5i\gamma \iint [\eta_S(\Delta\Omega, L) - \eta^*_I(\Delta\Omega, L)]\tilde{E}_S(\omega_1, 0)\tilde{E}^*_S(\omega_2, 0) \tilde{E}_S(\omega - \omega_1 + \omega_2, 0)d\omega_1 d\omega_2, \tag{6.24}$$

$$\delta_{NL,res} = i\gamma \iint \eta_{res}(\Delta\Omega, L)\tilde{E}_S(\omega_1, 0)\tilde{E}^*_S(\omega_2, 0) \tilde{E}_S(\omega - \omega_1 + \omega_2, 0)d\omega_1 d\omega_2, \tag{6.25}$$

where $\eta_{res}(\Delta\Omega, L) = 0.5[\eta_S(\Delta\Omega, L) - \eta^*_I(\Delta\Omega, L)]$ is the effective link transfer function after the nonlinear compensation in the PSA. Assuming the signal and idler experience the same link transfer function, i.e., $\eta_S(\Delta\Omega, L) = \eta_I(\Delta\Omega, L)$,

$$\begin{aligned} \eta_{res}(\Delta\Omega, L) &= 0.5[\eta_S(\Delta\Omega, L) - \eta_S(\Delta\Omega, L)^*] \\ &= iIm(\eta_S(\Delta\Omega, L)). \end{aligned} \tag{6.26}$$

PSA will cancel the distortions caused by the real part of the link transfer function but not the imaginary part.

Assuming PSA as a bulk optical amplifier with inline dispersion compensation, $D(z) = \beta_2 z - D_0$, where D_0 is the amount of inline pre-dispersion compensation. Then, the link transfer function (6.18) is given as [112],

$$\eta_S(\Delta\Omega, L) = \int_0^L \exp[G(z) + j\Delta\Omega(\beta_2 z - D_0)]dz. \tag{6.27}$$

Expanding the above equation,

$$\eta_S(\Delta\Omega, L) = \frac{1 - \exp(-\alpha L + i\Delta\Omega\beta_2 L)}{\alpha - i\Delta\Omega\beta_2} \exp(-i\Delta\Omega D_0). \tag{6.28}$$

The residual nonlinear distortion after nonlinear compensation in a PSA link where the signal and idler experiences the same link transfer function is

$$\eta_{res}(\Delta\Omega, L) = iIm\{\frac{1 - \exp(-\alpha L + i\Delta\Omega\beta_2 L)}{\alpha - i\Delta\Omega\beta_2} \exp(-i\Delta\Omega D_0)\}. \tag{6.29}$$

The dispersion pre-compensation, D_0, causes phase rotation that can reduce the residual nonlinear distortion. This has been studied as pre-dispersion compensation optimization to improve the transmission performance in [95, 113]. $\Delta\Omega$ is the range of ω_1 and ω_2 for which the $\tilde{E}_S(\omega_1, 0)$ and $\tilde{E}_S(\omega_2, 0)$ are nonzero, i.e., the optical bandwidth of the signal. For different values of $\Delta\Omega$, different D_0 is required to reduce the residual nonlinear distortion which is done by pre-dispersion optimization. As the optical bandwidth of the signal increases, the residual nonlinear distortion increases even with optimal pre-dispersion optimization which as been seen in paper A-C. Moreover, with $\alpha = 0$, i.e., by using ideal DRA and D_0 is 50%, the residual nonlinear distortion can be made zero. However, ideal DRA is difficult to achieve, the simplest of DRA is the backward pumping scheme which is also used in paper B. The above analysis can be extended easily to multi-span link assuming the nonlinear distortion from each span is the same as there is no accumulated dispersion in each of the span. Therefore, the nonlinear distortions add in-phase and the electric field of a link with N spans is

$$\tilde{E}_S(t, NL) = \tilde{E}_S(t, 0) + N\delta_{NL,res}(t, L). \tag{6.30}$$

One way to compensate the residual distortion in the multi-span link is to choose different D_0 for each span such that the residual nonlinear distortion from one span cancels the other. This has been demonstrated in [114, 115].

Modified third-order VNLE

Another way to compensate the residual nonlinear distortion is to use a modified VNLE as shown in Paper A. In the PSA link, with inline dispersion compensation and optical amplification, the first order Kernel from (6.3) can be modified as

$$K_1(\omega, z) = 1, \tag{6.31}$$

PSA has already removed the nonlinear distortion due to the real part of the link transfer function and now the third-order Kernel, K_3 have to just compensate for the residual nonlinear distortion after the PSA. Therefore, (6.4) becomes

$$K_3(\Delta\Omega, z) = iIm\{\frac{1 - \exp(-\alpha L + i\Delta\Omega\beta_2 L)}{\alpha - i\Delta\Omega\beta_2}\exp(-i\Delta\Omega D_0)\}. \tag{6.32}$$

With inline dispersion compensation, there is no accumulation of dispersion in each span and the nonlinear distortions in each span are more or less the same. Therefore, $F(\Delta\Omega)$ becomes equal to the number of spans to account for the same nonlinear distortions over all the spans.

Chapter 7

Summary of papers

This thesis is about the nonlinearity mitigation in phase-sensitively amplified links. In fiber-optic communication, the reach or throughput is mainly limited by the noise added in the optical amplifier and the nonlinear distortions caused by the Kerr effect in the optical fiber. Phase-sensitive amplifiers (PSAs) have a quantum-limited noise figure of 0 dB, as shown in section 5.3 compared to a 3 dB for the Phase-insensitive amplifier (PIA). As discussed in section 5.4.1, the copier-PSA implementation with a two-mode PSA can provide a 6 dB better link noise figure compared to using a phase-insensitively amplified link in the linear transmission regime. Moreover, the copier-PSA scheme is also capable of mitigating Kerr nonlinear distortions due to the coherent superposition of the signal and the conjugated copy of the signal called the idler in the PSA. Though lot of experiments have been performed to verify the nonlinearity mitigation using PSAs, no complete analytic analysis has been done.

In paper A, a thorough investigation has been done analytically on the nonlinearity mitigation in PSAs, similar to chapter 6. Using perturbation theory, a residual nonlinear distortion has been established when PSA mitigates nonlinearity using the copier-PSA implementation in single- or multi-span links. The residual nonlinear distortion for a copier-PSA link where the signal and idler experiences the same link transfer function depends only on imaginary part of the link transfer function as PSAs cancel out the nonlinear distortions caused by the real part. The investigation also shows the dependence of nonlinearity mitigation using PSAs on the involved optical bandwidth, dispersion map and power map. Finally, a modified VNLE with less computational

effort is proposed to compensate for the residual nonlinear distortion after nonlinear compensation in the PSA. The investigation was verified with numerical simulations using a 10 GBaud, 28 GBaud and 50 GBaud signals. The residual nonlinear distortion was minimized for each configuration with the dispersion map optimization. As the symbol rate was increased, the residual nonlinear distortion after PSA also increases, reducing the reach improvement when using a PSA compared to a PIA. Also, the VNLE was found to be more effective in mitigating the residual nonlinear distortions, especially at higher symbol rates.

In paper B, the optical bandwidth dependence on nonlinearity mitigation in PSAs is studied by comparing a 10 GBaud signal and a 28 GBaud signal in a multi-span link. The reach improvement from using PSA compared to PIA was 5 times for the 10 GBaud signal and 3.4 times for the 28 GBaud signal, showing that the effectiveness of nonlinearity mitigation in PSAs decreases with increasing symbol rate. As per the analytical investigation, adding distributed Raman amplification should increase the efficiency of nonlinearity mitigation in PSAs. This was also demonstrated with the 10 GBaud signal the reach improvement for PSA compared to PIA increased to 5.3 times. However, for the 28 GBaud signal, due to the experimental limitations, such an increase was not observed.

In paper C, three wavelength-division multiplexed (WDM) channels were used to study the efficacy of nonlinear mitigation in a PSA link. In a multi-span link, one, two and three 10 GBaud channels with a 12.5 GHz spacing were used in both simulations and experiments. As the number of channels was increased, the reach and optimal launch power decreased for both PIA and PSA systems. It was also found that PSAs can mitigate SPM better than XPM.

In paper D, wavelength-division multiplexed (WDM) system was used to study the cross-phase modulation (XPM) mitigation in a single-span PSA link. Two 10 GBaud channels spaced 25 GHz apart was used to study the mitigation of SPM and XPM separately in a PSA link. This is to our knowledge, the first demonstration of XPM mitigation in a PSA amplified link. In the simulations, PSA was found to mitigate SPM better compared to XPM. However, the SPM and XPM mitigation has similar performance in the experiments. Also, three 10 GBaud channels spaced 12.5 GHz apart were used to obtain a 9.5 dB allowable span loss increase using PSA compared to PIA for the center channel.

References

[1] C. W. Paper, "Cisco VNI global IP traffic forecast, 2017-2022," 2018. [Online]. Available: https://newsroom.cisco.com/press-release-content?type=webcontent&articleId=1955935

[2] A. G. Bell, "Apparatus for signalling and communicating, called photophone," Patent 235,199, 1880.

[3] T. H. Maiman, "Stimulated optical radiation in ruby," *Nature*, no. 4736, pp. 493–494, 1960.

[4] S. Miller and L. Tillotson, "Optical transmission research," *Applied optics*, vol. 5, no. 10, pp. 1538–1549, 1966.

[5] K. C. Kao and G. A. Hockham, "Dielectric-fibre surface waveguides for optical frequencies," *Proceedings of the Institution of Electrical Engineers*, vol. 113, no. 7, pp. 1151–1158, 1966.

[6] F. Kapron, D. B. Keck, and R. D. Maurer, "Radiation losses in glass optical waveguides," *Applied Physics Letters*, vol. 17, no. 10, pp. 423–425, 1970.

[7] T. Miya, Y. Terunuma, T. Hosaka, and T. Miyashita, "Ultimate low-loss single-mode fibre at 1.55 μm," *Electronics Letters*, vol. 15, no. 4, pp. 106–108, 1979.

[8] S. Poole, D. Payne, R. Mears, M. Fermann, and R. Laming, "Fabrication and characterization of low-loss optical fibers containing rare-earth ions," *Journal of Lightwave Technology*, vol. 4, no. 7, pp. 870–876, July 1986.

[9] L. Gruner-Nielsen, M. Wandel, P. Kristensen, C. Jorgensen, L. V. Jorgensen, B. Edvold, B. Palsdottir, and D. Jakobsen, "Dispersion-compensating fibers," *Journal of Lightwave Technology*, vol. 23, no. 11, pp. 3566–3579, 2005.

[10] K. O. Hill and G. Meltz, "Fiber bragg grating technology fundamentals and overview," *Journal of Lightwave Technology*, vol. 15, no. 8, pp. 1263–1276, 1997.

[11] Z. Tong, C. Lundström, P. Andrekson, C. McKinstrie, M. Karlsson, D. Blessing, E. Tipsuwannakul, B. Puttnam, H. Toda, and L. Grüner-Nielsen, "Towards ultrasensitive optical links enabled by low-noise phase-sensitive amplifiers," *Nature Photonics*, vol. 5, no. 7, pp. 430–436, 2011.

[12] P. Minzioni, "Nonlinearity compensation in a fiber-optic link by optical phase conjugation," *Fiber and Integrated Optics*, vol. 28, no. 3, pp. 179–209, 2009. [Online]. Available: https://doi.org/10.1080/01468030802364117

[13] X. Liu, A. Chraplyvy, P. Winzer, R. Tkach, and S. Chandrasekhar, "Phase-conjugated twin waves for communication beyond the kerr nonlinearity limit," *Nature Photonics*, vol. 7, no. 7, pp. 560–568, 2013.

[14] E. Ip and J. M. Kahn, "Compensation of dispersion and nonlinear impairments using digital backpropagation," *Journal of Lightwave Technology*, vol. 26, no. 20, pp. 3416–3425, 2008. [Online]. Available: http://jlt.osa.org/abstract.cfm?URI=jlt-26-20-3416

[15] K. V. Peddanarappagari and M. Brandt-Pearce, "Volterra series transfer function of single-mode fibers," *Journal of Lightwave Technology*, vol. 15, no. 12, pp. 2232–2241, 1997.

[16] Y. Tamura, H. Sakuma, K. Morita, M. Suzuki, Y. Yamamoto, K. Shimada, Y. Honma, K. Sohma, T. Fujii, and T. Hasegawa, "The first 0.14-dB/km loss optical fiber and its impact on submarine transmission," *Journal of Lightwave Technology*, vol. 36, no. 1, pp. 44–49, 2018.

[17] F. Yaman, Q. Lin, S. Radic, and G. P. Agrawal, "Impact of dispersion fluctuations on dual-pump fiber-optic parametric amplifiers," *IEEE Photonics Technology Letters*, vol. 16, no. 5, pp. 1292–1294, 2004.

[18] M. Karlsson, "Four-wave mixing in fibers with randomly varying zero-dispersion wavelength," *Journal of the Optical Society of America B*, vol. 15, no. 8, pp. 2269–2275, 1998.

[19] P. Velanas, A. Bogris, and D. Syvridis, "Impact of dispersion fluctuations on the noise properties of fiber optic parametric amplifiers," *Journal of lightwave technology*, vol. 24, no. 5, pp. 2171–2178, 2006.

[20] C. D. Poole and R. E. Wagner, "Phenomenological approach to polarisation dispersion in long single-mode fibres," *Electronics Letters*, vol. 22, no. 19, pp. 1029–1030, 1986.

[21] J. K. LL.D., "XL. a new relation between electricity and light: Dielectrified media birefringent," *The London, Edinburgh, and Dublin Philosophical Magazine and Journal of Science*, vol. 50, no. 332, pp. 337–348, 1875.

[22] ——, "LIV. a new relation between electricity and light: Dielectrified media birefringent (second paper)," *The London, Edinburgh, and Dublin Philosophical Magazine and Journal of Science*, vol. 50, no. 333, pp. 446–458, 1875.

[23] G. P. Agrawal, *Nonlinear Fiber Optics*, 5th ed. Academic Press, 2013.

[24] T. Nakanishi, M. Hirano, T. Okuno, and M. Onishi, "Silica-based highly nonlinear fiber with $\gamma = 30/\mathrm{W/km}$ and its FWM-based conversion efficiency," in *Optical Fiber Communication Conference*, 2006.

[25] R. H. Stolen and C. Lin, "Self-phase-modulation in silica optical fibers," *Physical Review A*, vol. 17, pp. 1448–1453, 1978. [Online]. Available: https://link.aps.org/doi/10.1103/PhysRevA.17.1448

[26] A. Hasegawa and F. Tappert, "Transmission of stationary nonlinear optical pulses in dispersive dielectric fibers. I. Anomalous dispersion," *Applied Physics Letters*, vol. 23, no. 3, pp. 142–144, 1973.

[27] L. F. Mollenauer, R. H. Stolen, and J. P. Gordon, "Experimental observation of picosecond pulse narrowing and solitons in optical fibers," *Physical Review Letters*, vol. 45, no. 13, pp. 1095–1098, 1980.

[28] A. Bononi, P. Serena, N. Rossi, and D. Sperti, "Which is the dominant nonlinearity in long-haul PDM-QPSK coherent transmissions?" in *European Conference on Optical Communication*, 2010.

[29] N. Rossi, P. Serena, and A. Bononi, "Symbol-rate dependence of dominant nonlinearity and reach in coherent WDM links," *Journal of Lightwave Technology*, vol. 33, no. 14, pp. 3132–3143, 2015.

[30] M. Karlsson, "Transmission systems with low noise phase-sensitive parametric amplifiers," *Journal of Lightwave Technology*, vol. 34, no. 5, pp. 1411–1423, 2016.

[31] R. Y. Chiao, C. H. Townes, and B. P. Stoicheff, "Stimulated Brillouin scattering and coherent generation of intense hypersonic waves," *Physical Review Letters*, vol. 12, pp. 592–595, 1964. [Online]. Available: https://link.aps.org/doi/10.1103/PhysRevLett.12.592

[32] E. Ippen and R. Stolen, "Stimulated brillouin scattering in optical fibers," *Applied Physics Letters*, vol. 21, no. 11, pp. 539–541, 1972. [Online]. Available: https://doi.org/10.1063/1.1654249

[33] K. O. Hill, B. S. Kawasaki, and D. C. Johnson, "CW brillouin laser," *Applied Physics Letters*, vol. 28, no. 10, pp. 608–609, 1976. [Online]. Available: https://doi.org/10.1063/1.88583

[34] S. P. Smith, F. Zarinetchi, and S. Ezekiel, "Narrow-linewidth stimulated Brillouin fiber laser and applications," *Optics Letters*, vol. 16, no. 6, pp. 393–395, 1991. [Online]. Available: http://ol.osa.org/abstract.cfm?URI=ol-16-6-393

[35] A. Almaiman, Y. Cao, M. Ziyadi, A. Mohajerin-Ariaei, P. Liao, C. Bao, F. Alishahi, A. Fallahpour, B. Shamee, N. Ahmed, A. J. Willner, Y. Akasaka, T. Ikeuchi, S. Takasaka, R. Sugizaki, S. Wilkinson, J. D. Touch, M. Tur, and A. E. Willner, "Experimental demonstration of phase-sensitive regeneration of a binary phase-shift keying channel without a phase-locked loop using Brillouin amplification," *Optics Letters*, vol. 41, no. 23, pp. 5434–5437, 2016. [Online]. Available: http://ol.osa.org/abstract.cfm?URI=ol-41-23-5434

[36] A. Almainman, Y. Cao, M. Ziyadi, A. Mohajerin-Ariaei, P. Liao, C. Bao, F. Alishahi, A. Fallahpour, B. Shamee, J. Touch, Y. Akasaka, T. Ikeuchi, S. Wilkinson, M. Tur, and A. E. Willner, "Experimental demonstration of phase-sensitive regeneration of a 20-40Gb/s QPSK channel without phase-locked loop using

Brillouin amplification," in *European Conference on Optical Communication*, 2016.

[37] Y. Cao, A. Almaiman, M. Ziyadi, P. Liao, A. Mohajerin-Ariaei, F. Alishahi, C. Bao, A. Falahpour, B. Shamee, A. Willner, Y. Akasaka, T. Ikeuchi, S. Wilkinson, J. Touch, M. Tur, and A. E. Willner, "Demonstration of automatically phase-locked self-homodyne detection with a low-power pilot tone based on Brillouin amplification and optical frequency combs," in *Optical Fiber Communication Conference*, 2016. [Online]. Available: http://www.osapublishing.org/abstract.cfm?URI=OFC-2016-M2A.6

[38] A. Lorences-Riesgo, M. Mazur, T. A. Eriksson, P. A. Andrekson, and M. Karlsson, "Self-homodyne 24x32-QAM superchannel receiver enabled by all-optical comb regeneration using Brillouin amplification," *Optics Express*, vol. 24, no. 26, pp. 29 714–29 723, 2016. [Online]. Available: http://www.opticsexpress.org/abstract.cfm?URI=oe-24-26-29714

[39] R. Engelbrecht, "Analysis of SBS gain shaping and threshold increase by arbitrary strain distributions," *Journal of Lightwave Technology*, vol. 32, no. 9, pp. 1689–1700, 2014.

[40] T. Nakanishi, M. Tanaka, T.Hasegawa, M. Hirano, T. Okuno, and M. Onishi, "$Al_2O_3 - SiO_2$ core highly nonlinear dispersion-shifted fiber with Brillouin gain suppression improved by 6.1dB," in *European Conference on Optical Communication*, 2006.

[41] Y. Takushima and T. Okoshi, "Suppression of stimulated Brillouin scattering using optical isolators," *Electronics Letters*, vol. 28, no. 12, pp. 1155–1157, 1992.

[42] D. Cotter, "Suppression of stimulated brillouin scattering during transmission of high-power narrowband laser light in monomode fibre," *Electronics Letters*, vol. 18, no. 15, pp. 638–640, 1982.

[43] J. Hansryd and P. A. Andrekson, "Broad-band continuous-wave-pumped fiber optical parametric amplifier with 49-dB gain and wavelength-conversion efficiency," *IEEE Photonics Technology Letters*, vol. 13, no. 3, pp. 194–196, 2001.

[44] A. Mussot, M. L. Parquier, and P. Szriftgiser, "Thermal noise for SBS suppression in fiber optical parametric amplifiers," *Optics Communications*, vol. 283, no. 12, pp. 2607 – 2610, 2010.

[45] M.-C. Ho and K. Y. K. Wong, "Narrow-linewidth idler generation in fiber four-wave mixing and parametric amplification by dithering two pumps in opposition of phase," *Journal of Lightwave Technology*, vol. 20, no. 3, pp. 469–476, 2002. [Online]. Available: http://jlt.osa.org/abstract.cfm?URI=jlt-20-3-469

[46] N. Yoshizawa and T. Imai, "Stimulated Brillouin scattering suppression by means of applying strain distribution to fiber with cabling," *Journal of Lightwave Technology*, vol. 11, no. 10, pp. 1518–1522, 1993.

[47] M. Takahashi, M. Tadakuma, and T. Yagi, "Dispersion and Brillouin managed HNLFs by strain control techniques," *Journal of Lightwave Technology*, vol. 28, no. 1, pp. 59–64, 2010.

[48] J. M. C. Boggio, J. D. Marconi, and H. L. Fragnito, "Experimental and numerical investigation of the SBS-threshold increase in an optical fiber by applying strain distributions," *Journal of Lightwave Technology*, vol. 23, no. 11, pp. 3808–3814, 2005.

[49] J. Hansryd, F. Dross, M. Westlund, P. A. Andrekson, and S. N. Knudsen, "Increase of the SBS threshold in a short highly nonlinear fiber by applying a temperature distribution," *Journal of Lightwave Technology*, vol. 19, no. 11, pp. 1691–1697, 2001.

[50] M. R. Lorenzen, D. Noordegraaf, C. V. Nielsen, O. Odgaard, L. Gruner-Nielsen, and K. Rottwitt, "Suppression of Brillouin scattering in fibre-optical parametric amplifier by applying temperature control and phase modulation," *Electronics Letters*, vol. 45, no. 2, pp. 125–126, 2009.

[51] B. P.-P. Kuo, J. M. Fini, L. Grüner-Nielsen, and S. Radic, "Dispersion-stabilized highly-nonlinear fiber for wideband parametric mixer synthesis," *Optics Express*, vol. 20, no. 17, pp. 18 611–18 619, 2012. [Online]. Available: http://www.opticsexpress.org/abstract.cfm?URI=oe-20-17-18611

[52] C. Lundström, R. Malik, L. Gruner-Nielsen, B. Corcoran, S. L. I. Olsson, M. Karlsson, and P. A. Andrekson, "Fiber optic parametric amplifier with 10-dB net gain without pump dithering," *IEEE Photonics Technology Letters*, vol. 25, no. 3, pp. 234–237, 2013.

[53] C. Huang, X. Guo, X. Fu, L. Wang, and C. Shu, "Active control of gain saturation in fiber-optical parametric amplifier using stimulated Brillouin scattering," *Optics Letters*, vol. 39, no. 19, pp. 5713–5716, 2014. [Online]. Available: http://ol.osa.org/abstract.cfm?URI=ol-39-19-5713

[54] L. Wang and C. Shu, "Dynamic control of gain profile in fiber-optical parametric amplifier by gain-transparent SBS," *IEEE Photonics Technology Letters*, vol. 25, no. 20, pp. 1996–1999, 2013.

[55] E. Mateo, F. Yaman, and G. Li, "Control of four-wave mixing phase-matching condition using the Brillouin slow-light effect in fibers," *Optics Letters*, vol. 33, no. 5, pp. 488–490, 2008. [Online]. Available: http://ol.osa.org/abstract.cfm?URI=ol-33-5-488

[56] L. Wang and C. Shu, "Dynamic control of phase matching in four-wave mixing wavelength conversion of amplitude- and phase- modulated signals," *Journal of Lightwave Technology*, vol. 31, no. 9, pp. 1468–1474, 2013. [Online]. Available: http://jlt.osa.org/abstract.cfm?URI=jlt-31-9-1468

[57] C. V. Raman and K. S. Krishnan, "A new type of secondary radiation," *Nature*, vol. 121, no. 11, pp. 501–502, 1928.

[58] E. Woodbury and W. Ng, "Ruby laser operation in near IR," *Proceedings of the Institute of Radio Engineers*, vol. 50, no. 11, pp. 2347–2348, 1962.

[59] M.-C. Ho, K. Uesaka, M. Marhic, and Y. Akasaka, "200-nm-bandwidth fiber optical amplifier combining parametric and Raman gain," *Journal of Lightwave Technology*, vol. 19, no. 7, pp. 977–981, 2001. [Online]. Available: http://jlt.osa.org/abstract.cfm?URI=jlt-19-7-977

[60] M. Stephens, I. Phillips, P. Rosa, P. Harper, and N. Doran, "Improved WDM performance of a fibre optical parametric amplifier using Raman-assisted pumping," *Optics Express*,

vol. 23, no. 2, pp. 902–911, 2015. [Online]. Available: http://www.opticsexpress.org/abstract.cfm?URI=oe-23-2-902

[61] Z. Tong, A. Bogris, M. Karlsson, and P. A. Andrekson, "Full characterization of the signal and idler noise figure spectra in single-pumped fiber optical parametric amplifiers," *Optics Express*, vol. 18, no. 3, pp. 2884–2893, 2010. [Online]. Available: http://www.opticsexpress.org/abstract.cfm?URI=oe-18-3-2884

[62] G. P. Agrawal, *Fiber-Optic Communication Systems*, 4th ed. John Wiley & Sons, 2010.

[63] C. M. Caves, "Quantum limits on noise in linear amplifiers," *Phys. Rev. D*, vol. 26, pp. 1817–1839, 1982. [Online]. Available: https://link.aps.org/doi/10.1103/PhysRevD.26.1817

[64] F. A. Flood, "L-band erbium-doped fiber amplifiers," in *Optical Fiber Communication Conference*, 2000.

[65] J. Bromage, "Raman amplification for fiber communications systems," *Journal of Lightwave Technology*, vol. 22, no. 1, pp. 79–93, 2004. [Online]. Available: http://jlt.osa.org/abstract.cfm?URI=jlt-22-1-79

[66] R. I. Laming, M. N. Zervas, and D. N. Payne, "Erbium-doped fiber amplifier with 54 dB gain and 3.1 dB noise figures," *IEEE Photonics Technology Letters*, vol. 4, no. 12, pp. 1345–1347, 1992.

[67] A. E. Kelly, I. F. Lealman, L. J. Rivers, S. D. Perrin, and M. Silver, "Low noise figure (7.2 dB) and high gain (29 dB) semiconductor optical amplifier with a single layer AR coating," *Electronics Letters*, vol. 33, no. 6, pp. 536–538, 1997.

[68] X. Li and G. Li, "Electrical post-compensation of SOA impairments for fiber-optic transmission," *IEEE Photonics Technology Letters*, vol. 21, no. 9, pp. 581–583, 2009.

[69] M. N. Islam, "Raman amplifiers for telecommunications," *IEEE Journal of Selected Topics in Quantum Electronics*, vol. 8, no. 3, pp. 548–559, 2002.

[70] E. Desurvire, M. Papuchon, J. P. Pocholle, J. Raffy, and D. B. Ostrowsky, "High-gain optical amplification of laser diode signal

by Raman scattering in single-mode fibres," *Electronics Letters*, vol. 19, no. 19, pp. 751–753, 1983.

[71] E. Pincemin, T. Guillossou, N. Evanno, S. Lobanov, and S. Ten, "Record transmission distances over ultra low loss G.652 fibre with NRZ-OOK or NRZ-DPSK 40 Gbps WDM systems," in *Optical Fiber Communication*, 2009.

[72] C. Headley and G. Agrawal, *Raman amplification in fiber optical communication systems*. Academic press, 2005.

[73] H. T. Friis, "Noise figures of radio receivers," *Proceedings of the Institute of Radio Engineers*, vol. 32, no. 7, pp. 419–422, 1944.

[74] Z. Tong, C. J. McKinstrie, C. Lundström, M. Karlsson, and P. A. Andrekson, "Noise performance of optical fiber transmission links that use non-degenerate cascaded phase-sensitive amplifiers," *Optics Express*, vol. 18, no. 15, pp. 15 426–15 439, 2010. [Online]. Available: http://www.opticsexpress.org/abstract.cfm?URI=oe-18-15-15426

[75] S. J. Savory, G. Gavioli, R. I. Killey, and P. Bayvel, "Electronic compensation of chromatic dispersion using a digital coherent receiver," *Optics Express*, vol. 15, no. 5, pp. 2120–2126, 2007. [Online]. Available: http://www.opticsexpress.org/abstract.cfm?URI=oe-15-5-2120

[76] M. Wandel, T. Veng, N. T. Quang Le, and L. Gruner-Nielsen, "Dispersion compensating fibre with a high figure of merit," in *European Conference on Optical Communication*, 2001.

[77] E. Tipsuwannakul, J. Li, T. A. Eriksson, L. Egnell, F. Sjöström, J. Pejnefors, P. A. Andrekson, and M. Karlsson, "Influence of fiber-Bragg grating-induced group-delay ripple in high-speed transmission systems," *Journal of Optical Communications and Networking*, vol. 4, no. 6, pp. 514–521, 2012. [Online]. Available: http://jocn.osa.org/abstract.cfm?URI=jocn-4-6-514

[78] H. Bülow, F. Buchali, and A. Klekamp, "Electronic dispersion compensation," *Journal of Lightwave Technology*, vol. 26, no. 1, pp. 158–167, 2008. [Online]. Available: http://jlt.osa.org/abstract.cfm?URI=jlt-26-1-158

[79] M. E. Marhic, "Analytic solutions for the phases of waves coupled by degenerate or nondegenerate four-wave mixing," *Journal of the Optical Society of America B*, vol. 30, no. 1, pp. 62–70, 2013. [Online]. Available: http://josab.osa.org/abstract.cfm?URI=josab-30-1-62

[80] ——, *Fiber Optical Parametric Amplifiers, Oscillators and Related Devices*. Cambridge University Press, 2007.

[81] K. Inoue and T. Mukai, "Signal wavelength dependence of gain saturation in a fiber optical parametric amplifier," *Optics Letters*, vol. 26, no. 1, pp. 10–12, 2001. [Online]. Available: http://ol.osa.org/abstract.cfm?URI=ol-26-1-10

[82] C. J. McKinstrie and S. Radic, "Phase-sensitive amplification in a fiber," *Optics Express*, vol. 12, no. 20, pp. 4973–4979, 2004. [Online]. Available: http://www.opticsexpress.org/abstract.cfm?URI=oe-12-20-4973

[83] C. J. McKinstrie, S. Radic, and A. R. Chraplyvy, "Parametric amplifiers driven by two pump waves," *IEEE Journal of Selected Topics in Quantum Electronics*, vol. 8, no. 3, pp. 538–547, 2002.

[84] Y. Chen and A. W. Snyder, "Four-photon parametric mixing in optical fibers: effect of pump depletion," *Optics Letters*, vol. 14, no. 1, pp. 87–89, 1989. [Online]. Available: http://ol.osa.org/abstract.cfm?URI=ol-14-1-87

[85] J. Hansryd, P. A. Andrekson, M. Westlund, Jie Li, and P.-O. Hedekvist, "Fiber-based optical parametric amplifiers and their applications," *IEEE Journal of Selected Topics in Quantum Electronics*, vol. 8, no. 3, pp. 506–520, 2002.

[86] P. Kylemark, P. O. Hedekvist, H. Sunnerud, M. Karlsson, and P. A. Andrekson, "Noise characteristics of fiber optical parametric amplifiers," *Journal of Lightwave Technology*, vol. 22, no. 2, pp. 409–416, 2004.

[87] P. L. Voss, K. G. Köprülü, and P. Kumar, "Raman-noise-induced quantum limits for $\chi^{(3)}$ nondegenerate phase-sensitive amplification and quadrature squeezing," *Journal of the Optical Society of America B*, vol. 23, no. 4, pp. 598–610, 2006.

[88] M. E. Marhic, C. H. Hsia, and J. . Jeong, "Optical amplification in a nonlinear fibre interferometer," *Electronics Letters*, vol. 27, no. 3, pp. 210–211, 1991.

[89] W. Imajuku, A. Takada, and Y. Yamabayashi, "Inline coherent optical amplifier with noise figure lower than 3 dB quantum limit," *Electronics Letters*, vol. 36, no. 1, pp. 63–64, 2000.

[90] M. E. Marhic and C.-H. Hsia, "Optical amplification and squeezed-light generation in fibre interferometers performing degenerate four-wave mixing," *Quantum Optics: Journal of the European Optical Society Part B*, vol. 3, no. 6, pp. 341–358, 1991. [Online]. Available: https://doi.org/10.1088%2F0954-8998%2F3%2F6%2F004

[91] Z. Tong, A. Bogris, C. Lundström, C. J. McKinstrie, M. Vasilyev, M. Karlsson, and P. A. Andrekson, "Modeling and measurement of the noise figure of a cascaded non-degenerate phase-sensitive parametric amplifier," *Optics Express*, vol. 18, no. 14, pp. 14 820–14 835, 2010. [Online]. Available: http://www.opticsexpress.org/abstract.cfm?URI=oe-18-14-14820

[92] C. J. McKinstrie, S. Radic, and M. G. Raymer, "Quantum noise properties of parametric amplifiers driven by two pump waves," *Optics Express*, vol. 12, no. 21, pp. 5037–5066, 2004. [Online]. Available: http://www.opticsexpress.org/abstract.cfm?URI=oe-12-21-5037

[93] R. Malik, A. Kumpera, A. Lorences-Riesgo, P. A. Andrekson, and M. Karlsson, "Frequency-resolved noise figure measurements of phase (in)sensitive fiber optical parametric amplifiers," *Optics Express*, vol. 22, no. 23, pp. 27 821–27 832, 2014. [Online]. Available: http://www.opticsexpress.org/abstract.cfm?URI=oe-22-23-27821

[94] C. J. McKinstrie, M. Karlsson, and Z. Tong, "Field-quadrature and photon-number correlations produced by parametric processes," *Optics Express*, vol. 18, no. 19, pp. 19 792–19 823, 2010. [Online]. Available: http://www.opticsexpress.org/abstract.cfm?URI=oe-18-19-19792

[95] S. L. Olsson, M. Karlsson, and P. A. Andrekson, "Nonlinear phase noise mitigation in phase-sensitive amplified transmission systems," *Optics Express*, vol. 23, no. 9, pp. 11 724–11 740, 2015. [Online]. Available: http://www.opticsexpress.org/abstract.cfm?URI=oe-23-9-11724

[96] B. Corcoran, R. Malik, S. L. I. Olsson, C. Lundström, M. Karlsson, and P. A. Andrekson, "Noise beating in hybrid phase-sensitive amplifier systems," *Optics Express*, vol. 22, no. 5, pp. 5762–5771, 2014. [Online]. Available: http://www.opticsexpress.org/abstract.cfm?URI=oe-22-5-5762

[97] A. Durecu-Legrand, C. Simonneau, D. Bayart, A. Mussot, T. Sylvestre, E. Lantz, and H. Maillotte, "Impact of pump osnr on noise figure for fiber-optical parametric amplifiers," *IEEE Photonics Technology Letters*, vol. 17, no. 6, pp. 1178–1180, 2005.

[98] R. Kakarla, J. Schröder, and P. A. Andrekson, "Optical injection locking at sub nano-watt powers," *Optics Letters*, vol. 43, no. 23, pp. 5769–5772, 2018. [Online]. Available: http://ol.osa.org/abstract.cfm?URI=ol-43-23-5769

[99] S. Olsson, H. Eliasson, E. Astra, M. Karlsson, and P. Andrekson, "Long-haul optical transmission link using low-noise phase-sensitive amplifiers." *Nature communications*, vol. 9, no. 1, pp. 2513–2513, 2018.

[100] R. Essiambre, G. Kramer, P. J. Winzer, G. J. Foschini, and B. Goebel, "Capacity limits of optical fiber networks," *Journal of Lightwave Technology*, vol. 28, no. 4, pp. 662–701, 2010.

[101] A. D. Ellis, J. Zhao, and D. Cotter, "Approaching the non-linear shannon limit," *Journal of Lightwave Technology*, vol. 28, no. 4, pp. 423–433, Feb 2010. [Online]. Available: http://jlt.osa.org/abstract.cfm?URI=jlt-28-4-423

[102] R. Essiambre and R. W. Tkach, "Capacity trends and limits of optical communication networks," *Proceedings of the IEEE*, vol. 100, no. 5, pp. 1035–1055, 2012.

[103] E. Agrell, "Nonlinear fiber capacity," in *European Conference on Optical Communication*, 2013.

[104] J. P. Gordon and L. F. Mollenauer, "Phase noise in photonic communications systems using linear amplifiers," *Optics Letters*, vol. 15, no. 23, pp. 1351–1353, 1990. [Online]. Available: http://ol.osa.org/abstract.cfm?URI=ol-15-23-1351

[105] J. C. Cartledge, F. P. Guiomar, F. R. Kschischang, G. Liga, and M. P. Yankov, "Digital signal processing for fiber nonlinearities," *Optics Express*, vol. 25, no. 3, pp. 1916–1936, 2017.

[106] S. L. I. Olsson, B. Corcoran, C. Lundström, M. Sjödin, M. Karlsson, and P. A. Andrekson, "Phase-sensitive amplified optical link operating in the nonlinear transmission regime," in *European Conference on Optical Communication*, 2012.

[107] F. P. Guiomar, J. D. Reis, A. L. Teixeira, and A. N. Pinto, "Mitigation of intra-channel nonlinearities using a frequency-domain Volterra series equalizer," *Optics Express*, vol. 20, no. 2, pp. 1360–1369, 2012.

[108] F. P. Guiomar and A. N. Pinto, "Simplified Volterra series nonlinear equalizer for polarization-multiplexed coherent optical systems," *Journal of Lightwave Technology*, vol. 31, no. 23, pp. 3879–3891, 2013.

[109] Y. Tian, Y.-K. Huang, S. Zhang, P. R. Prucnal, and T. Wang, "Demonstration of digital phase-sensitive boosting to extend signal reach for long-haul WDM systems using optical phase-conjugated copy," *Optics Express*, vol. 21, no. 4, pp. 5099–5106, 2013. [Online]. Available: http://www.opticsexpress.org/abstract.cfm?URI=oe-21-4-5099

[110] H. Eliasson, P. Johannisson, M. Karlsson, and P. A. Andrekson, "Mitigation of nonlinearities using conjugate data repetition," *Optics Express*, vol. 23, no. 3, pp. 2392–2402, 2015.

[111] X. Liu, S. Chandrasekhar, A. Gnauck, P. Winzer, S. Randel, S. Corteselli, A. Chraplyvy, R. Tkach, B. Zhu, T. Taunay *et al.*, "Digital coherent superposition for performance improvement of spatially multiplexed coherent optical OFDM superchannels," *Optics Express*, vol. 20, no. 26, pp. B595–B600, 2012.

[112] H. Louchet, A. Hodzic, K. Petermann, A. Robinson, and R. Epworth, "Simple criterion for the characterization of nonlinear impairments in dispersion-managed optical transmission systems," *IEEE Photonics Technology Letters*, vol. 17, no. 10, pp. 2089–2091, 2005.

[113] B. Corcoran, S. L. I. Olsson, C. Lundström, M. Karlsson, and P. A. Andrekson, "Mitigation of nonlinear impairments on QPSK data in phase-sensitive amplified links," in *European Conference on Optical Communication*, 2013.

[114] E. Astra, S. L. I. Olsson, H. Eliasson, and P. A. Andrekson, "Dispersion management for nonlinearity mitigation in two-span 28 GBaud QPSK phase-sensitive amplifier links," *Optics Express*, vol. 25, no. 12, pp. 13 163–13 173, Jun 2017. [Online]. Available: http://www.opticsexpress.org/abstract.cfm?URI=oe-25-12-13163

[115] E. Astra, H. Eliasson, and P. A. Andrekson, "Four-span dispersion map optimization for improved nonlinearity mitigation in phase-sensitive amplifier links," in *European Conference on Optical Communication*, 2017.